NASA TECHNICAL
MEMORANDUM

NASA TM-78254

THE STRATIGRAPHIC SEQUENCE OF VOLCANIC AND SEDIMENTARY UNITS IN THE NORTH POLAR REGION OF MARS

By Michael E. Botts
Space Sciences Laboratory

January 1980

NASA

George C. Marshall Space Flight Center
Marshall Space Flight Center, Alabama

1. Report No NASA TM-78254	2. Government Accession No.	3. Recipient's Catalog No.
4. Title and Subtitle The Stratigraphic Sequence of Volcanic and Sedimentary Units in the North Polar Region of Mars		5. Report Date January 1980
		6. Performing Organization Code
7. Author(s) Michael E. Botts*		8. Performing Organization Report No.
9. Performing Organization Name and Address George C. Marshall Space Flight Center Marshall Space Flight Center, Alabama 35812		10. Work Unit No.
		11. Contract or Grant No.
12. Sponsoring Agency Name and Address National Aeronautics and Space Administration Washington, D. C. 20546		13. Type of Report and Period Covered Technical Memorandum
		14. Sponsoring Agency Code

15. Supplementary Notes
Prepared by Space Sciences Laboratory, Science and Engineering

*Universities Space Research Association

16. Abstract
Based on photogeologic mapping of Viking Orbiter images of Mars, four distinct informal stratigraphic units can be defined for the region north of 70°N latitude. They are: (a) bulbous plains, (b) mantled plains, (c) dune deposits, and (d) layered deposits/perennial ice.

The bulbous plains unit underlies all other north polar units and represents a sub-unit of the mottled cratered plains. Based on crater size-frequency data, bulbous plains is equivalent in age to the relatively old cratered plains unit at Tempe Plateau (90°W, 30°N). The low albedo of bulbous plains and the appearance of what appears to be a dike suggest that bulbous plains has a volcanic origin. Cumulative crater size-frequency distribution functions for bulbous and mantled plains display two-segment curves with a crater-production slope of -2.0 and a cratering-obliteration equilibrium slope of -0.7. This supports the interpretation that mantled plains were formed by dust blanketing of bulbous plains. As calculated from crater size-frequency distribution functions, the relative surface-obliteration rates are 1:9:88 for bulbous, moderately mantled, and heavily mantled plains, respectively.

The layered deposits probably represent a facies of mantled plains in which dust has been deposited onto the perennial ice cap rather than directly onto the ground. Thus, the areal extent of the layered deposits at the north and south poles may indicate the maximum extent of the perennial ice caps as controlled by changes in Martian orbital parameters.

Dune deposits occur in the form of longitudinal, transverse, and barchan dunes, and possibly as sheet sand deposits. Actual dunes are generally confined to mantled plains, suggesting that mantling provides a proper substratum for dune accumulation.

Surface winds for the north polar region were determined from dune orientations to flow predominantly counterclockwise around the polar cap, although there is evidence for dune modification by secondary winds spiralling clockwise off of the cap.

A gradation from densely spaced transverse dunes to more dispersed barchan and transverse dunes implies a general thinning of circumpolar dune deposits downwind of extensive areas mapped as bulbous plains. The author suggests that dune material is being stripped from bulbous plains and is accumulating as dunes downwind on mantled plains.

17. Key Words (Suggested by Author(s))		18. Distribution Statement
Mars Geology Sand Dunes North Pole	Aeolian Winds Crater Counts	Unclassified—Unlimited

19. Security Classif. (of this report)	20. Security Classif (of this page)	21. No. of Pages	22. Price
Unclassified	Unclassified	68	NTIS

MSFC - Form 3292-1 (Rev December 1972)   For sale by National Technical Information Service, Springfield, Virginia 22151

ACKNOWLEDGMENTS

TABLE OF CONTENTS

LIST OF FIGURES

SUMMARY

Based on photogeologic mapping of Viking Orbiter images of Mars, four distinct informal stratigraphic units can be defined for the region north of 70°N latitude. They are: (a) bulbous plains, (b) mantled plains, (c) dune deposits, and (d) layered deposits/perennial ice.

The bulbous plains unit underlies all other north polar units and represents a sub-unit of the mottled cratered plains. Based on crater size-frequency data, bulbous plains is equivalent in age to the relatively old cratered plains unit at Tempe Plateau (90°W, 30°N). The low albedo of bulbous plains and the appearance of what appears to be a dike suggest that bulbous plains has a volcanic origin. Cumulative crater size-frequency distribution functions for bulbous and mantled plains display two-segment curves with a crater-production slope of -2.0 and a cratering-obliteration equilibrium slope of -0.7. This supports the interpretation that mantled plains were formed by dust blanketing of bulbous plains. As calculated from crater size-frequency distribution functions, the relative surface-obliteration rates are 1:9:88 for bulbous, moderately mantled, and heavily mantled plains, respectively.

The layered deposits probably represent a facies of mantled plains in which dust has been deposited onto the perennial ice cap rather than directly onto the ground. Thus, the areal extent of the layered deposits at the north and south poles may indicate the maximum extent of the perennial ice caps as controlled by changes in Martian orbital parameters.

Dune deposits occur in the form of longitudinal, transverse, and barchan dunes, and possibly as sheet sand deposits. Actual dunes are generally confined to mantled plains, suggesting that mantling provides a proper substratum for dune accumulation.

Surface winds for the north polar region were determined from dune

2

orientations to flow predominantly counterclockwise around the polar cap,
although there is evidence for dune modification by secondary winds spiralling
clockwise off of the cap.

A gradation from densely spaced transverse dunes to more dispersed
barchan and transverse dunes implies a general thinning of circumpolar dune
deposits downwind of extensive areas mapped as bulbous plains. The author
suggests that dune material is being stripped from bulbous plains and is
accumulating as dunes downwind on mantled plains.

Telescopic Observations

Man first became interested in the polar regions of Mars when white polar spots were reported by Cassini in 1666 and again by Huygens in 1672. In 1784, Sir William Herschel studied the changing size of the polar caps with seasons and interpreted the polar spots as seasonal accumulations of ice and snow. The melting of the polar caps was found to be intimately related to the "wave of darkening" of the Martian surface during summer (1).

Although Wilhelm Beer and Johann Mädler reported the presence of a dark band around the receding north pole of Mars in 1830, little further attention was given to the observation until 1894 when Percival Lowell reported a similar band around the south polar cap. This sparked controversy as to whether the dark bands were real features of the Martian surface or just an optical illusion (2). Since the circumpolar bands were interpreted as moistened ground, their presence would imply actual melting of the retreating polar water ice rather than sublimation (1). Lowell envisioned his Martian "canals" as an irrigation system designed to bring water from the melting caps to the arid lower latitudes (2).

Two distinct types of Martian polar "caps" have been recognized since 1907. The spring and summer caps are surface deposits whereas the "caps" observed in autumn and winter are cloud mantles (i.e. the polar hood). The polar hood begins forming as the summer ends and disappears rather abruptly at vernal equinox (1).

Two major differences between the north and south polar ice caps have been recognized from telescopic observations. Whereas the north polar cap is centered almost precisely on the rotation axis of Mars, the center of the south polar cap deviates from the rotation axis by 5°. Also, the north polar

cap is larger than the southern cap, probably due to the fact that the subsolar latitude during perihelion is presently in the southern hemisphere. It is probable that during this period of excess insolation in the southern hemisphere, the north polar cap grows at the expense of the southern cap (3).

Mariner Mission Results

Neither polar cap was imaged by the 20 pictures returned by the Mariner 4 Mars flyby mission in 1965. However, spectrometry data taken during Mars occultation determined that the Martian atmosphere was essentially carbon dioxide at a few millibars. This led many to argue that the polar caps may also be primarily carbon dioxide (2).

The first "close-up" images of the south polar cap were taken by the Mariner 7 spacecraft as it flew by Mars in 1969. No dark circumpolar band was observed for the south polar region, placing serious doubt on the possibility that a dark "melt band" might occur around the north pole (2).

The Mariner 9 orbiting spacecraft photographed Mars from November 1971 to March 1972, and provided excellent south polar coverage. This was, in part, due to the fact that the south pole was the only feature clearly seen through the global dust storm which enshrouded Mars during the early mission, and because the orbit of the spacecraft traversed the south pole every revolution during the orbit's periapsis. The entire south pole was imaged at 3-4 km resolution with 20% covered by 300-400 m resolution (3).

One of the most striking features of the south pole is the "quasi-linear, swirl-like" pattern seen in the ice cap. The north polar cap was later found to display an even more pronounced swirl pattern (see figure 1). Based on Mariner 9 images, several mechanisms have been proposed to account for these features. Murray and Malin (4) proposed that the curvilinear features represented the edges of stacked plates of ice and suggested that an offsetting

of these plates provided evidence for polar wandering. Others believed the features represented troughs rather than the edges of plates, and suggested spiralling polar winds (5), or mass-wasting (6) as the dominant erosion mechanisms.

The excellent Mariner 9 coverage of the south polar region provided a clear understanding of its stratigraphic sequence (7). The ancient cratered terrain, which is the oldest unit on Mars and covers most of the southern hemisphere, underlies the south polar region as well. Massive (i.e. un-layered) blankets, probably composed of fine, wind-transported dust, overlie the ancient cratered terrain in the south polar region. These blankets have been extensively eroded to form pitted terrain and etched terrain (8). The massive blankets are overlain, sometimes unconformably, by layered deposits which have been subsequently eroded to expose the layering in troughs and scarps. In addition to the thin mantles of CO_2 ice which advance and retreat each year (7), permanent ice caps cover both poles though Mariner 9 investigations could not determine whether the permanent caps consist of H_2O or CO_2 ice.

The layered deposits probably form by cyclic deposition of wind-blown dust carried in from the mid-latitudes (9). Deposition models using 50,000 and 95,000 year climatic cycles have been proposed to account for the layers (4), although Cutts concludes that such a period is too short to allow transport of sufficient material to the poles. However, a 2 million-year cycle of orbital ellipticity of Mars may modify the intensity of global dust storms enough to cause the layering, and allow time for a sufficient amount of material to be transported to the poles (9).

Compared to the south polar coverage, Mariner 9 coverage of the north pole of Mars was relatively poor. Not only was the spacecraft's orbit much higher over the north pole compared to the orbital range during south polar

traverses, but the polar hood obscured the north polar region during most of the standard mission. Although visibility improved greatly during the Mariner 9 extended mission, north polar coverage was severely limited because of a shortage in the spacecraft's attitude-control gas.

Mariner 9 imagery products showed the north polar cap and its associated layered deposits to be very similar to deposits of the south pole. Minor differences include the more pronounced "swirl-like" pattern of the north polar cap and the greater extent of the northern permanent ice cap. Layered deposits in the north are more extensively covered by permanent ice than at the south pole.

Although the lack of a dark circumpolar band in the south had placed serious doubt on the presence of such a band in the north, a very low albedo band around the northern pole was confirmed by Mariner 9. However, the feature was found to be fixed in position, rather than a halo surrounding a retreating ice cap. Sagan et. al. (10) attributed the presence of the dark band to the scouring of a thin layer of bright dust by strong polar winds.

Mariner 9, for the first time, allowed determination of the stratigraphic sequence of the north polar region (11). Like the south polar region, the sequence in the north was found to include an underlying cratered unit, a massive deposit interpreted as wind-blown dust, and layered deposits capped by permanent ice.

However, the underlying moderately cratered unit is not the ancient cratered terrain, but rather a younger unit designated as mottled cratered plains. These plains are characterized by Soderblom et. al. (11) as having an abundance of small craters (10-20 km diameter), lower average albedo than most of Mars, and a highly mottled appearance which results from numerous bright and dark streaks and bright material highlighting crater rims and

interiors. As mapped by Soderblom et. al. the mottled cratered plains are distributed rather extensively between 55° to 80° north latitudes.

Overlying the mottled cratered plains is a bright debris mantle which was subdivided into smooth, etch-pitted, and rippled plains (11). Rippled and etched-pitted plains were interpreted as depositional and erosional modifications of smooth plains. Because of the severely limited extent and poor quality of the Mariner 9 north polar coverage, the geologic mapping of Soderblom et. al. (11) is labelled by the authors as "preliminary" and contains numerous implied boundaries between units.

Viking Mission Results (August 1976-November 1978)

Compared to Mariner 9, the Viking Orbiter spacecrafts, particularly VO2, provided much improved coverage of the north polar region of Mars. Following the successful landings of Viking Landers 1 and 2, the inclination of the orbit of Viking Orbiter 2 was changed from 55° to 75° in order to permit extensive north polar coverage before polar hood formation (33). Ground resolution of the north polar images taken with the VO2 in this orbit was 100-180 meters as compared to 300-400 meters for Mariner 9 high-resolution coverage of the south pole (3). During the extend Viking mission, the orbital inclination of VO2 was further increased to 80° and the periapsis lowered from 1500 km to 778 km (33). This improved the ground resolution of the north polar imagery to about 60 meters.

In addition to the Viking Orbiter imaging capabilities, the Orbiters included an infrared thermal mapper (IRTM) which provided conclusive evidence that the residual ice cap at the north pole was composed of a "dirty water ice" (12). Summer temperatures at the south pole have not dropped low enough to allow a similar determination of the composition of the south polar cap (34).

The spiral patterns within the polar caps have continued to intrigue Viking investigators. Although it is now generally accepted that these features are troughs rather than plate edges, there is still much controversy as to the origin of the troughs. As an alternate hypothesis to the rotating wind erosion and mass wasting processes mentioned earlier, Howard (13) has suggested that isolation-controlled ice ablation and accumulation could account for the spiral pattern of the troughs, with wind action only serving to redistribute dust across layered deposits.

The circumpolar dark band, which had been confirmed by Mariner 9 investigations, was determined from Viking images not to be a deflation feature as had been predicted earlier, but corresponded instead to large dune fields partially surrounding the north polar ice cap (14). It will be shown in this paper, however, that not all of the dark areas can be explained by the presence of visible dunes.

Determining the source of such a large supply of dune material has become a very intriguing problem. Any model attempting to define the source of the north polar dune deposits must consider: (a) the unique geographic association of large fields with the north polar region, (b) the very low albedo of the dune deposits ($A_L \leq 0.20$) (12), and (c) the particle size required for saltation in the Martian environment (diameter = 200-250 μm; 15). An added complication to the grain size requirement is that sands appear to be absent at the Viking Landing sites, possibly due to self-destruction of saltating grains during the impacts with rocks (i.e. the "kamikaze" effect; 16). Therefore, the model must account for sand-sized particles being present at high latitudes while apparently absent at lower latitudes. Source models proposed fall into three general categories: (a) dune sands have been transported from lower latitudes predominantly by saltation (14), (b) dune material consists of aggregates of atmospherically-derived dust, which have

been deposited either directly onto the ground as "dirty iceballs" (17), or onto the polar cap where it is subsequently eroded from the layered deposits (14), and (c) dune sands have a regional source implying processes unique to the north polar region (15, this paper). Each model proposed has certain problems which must be accounted for.

Blasius et. al. (35) have suggested that aeolian carving of many of the channels leading into Chryse Planitia may have supplied both suspended and saltating material to the northern plains. Although conditions may have been different in the past, neither wind streak data (3, 10) nor atmospheric models based on present corditions (18, 19) support such an atmospheric flow direction.

A major complication with the proposed atmospheric-dust models is that they require aggregation of fines to form sand-sized particles, using aggregate bonding mechanisms such as electrostatics (20), ice (17), or evaporites (14). A more serious problem is that the atmospheric-dust models fail to account for the low albedo of the dune deposits, since atmospheric dust on Mars is commonly known to have a high albedo.

A regional-source model must explain the uniqueness of the large supply of dune material in the north polar region, by assiming either a unique source unit, a unique polar process, or both. Squyres (15) has suggested that a regional source of "coarse-grained" basalt may produce low-albedo dune material which retains its sand-size and low albedo because of low UV weathering rates. Retention of an adequate sand supply may be aided by high mechanical weathering rates which result from freeze-thaw processes and glacial grinding.

Based on the improved coverage by the Viking Orbiter spacecrafts, Squyres (15) revised the stratigraphic sequence in the north polar region to include dune material. Following much the same sequence as set forth by Soderblom et. al.,

10

Squyres divided the stratigraphy into moderately-cratered plains material, debris mantle (massive deposits), dune material, laminated (layered) deposits, and perennial ice. Using results derived through photogeologic mapping and from crater size-frequency distribution data, it will be shown in this paper that the stratigraphic mapping of Squyres is inconsistent with his description of the units.

The results of the present paper were primarily obtained from photo-geologic mapping of Viking Orbiter imagery in the form of mosaics and individual enlarged frames. The goals of the research were (a) to redefine and map distinct informal stratigraphic units in the north polar region of Mars (i.e. > 70°N latitude), (b) to define and interpret crater size-frequency distribution functions for particular units, (c) to map the directions of dune-driving winds based on the orientation and form of circumpolar dunes, and (d) to infer a source for the north polar dune deposits based on the relationships between dune-driving winds and the distribution of stratigraphic units.

Figure 1: Mariner 9 mosaic of the north polar region of Mars (from Mars as Viewed from Mariner 9, NASA SP-329, 1976). Note the well developed spiral pattern within the ice cap. The low-albedo band surrounding the cap corresponds in part to the presence of dune fields.

12
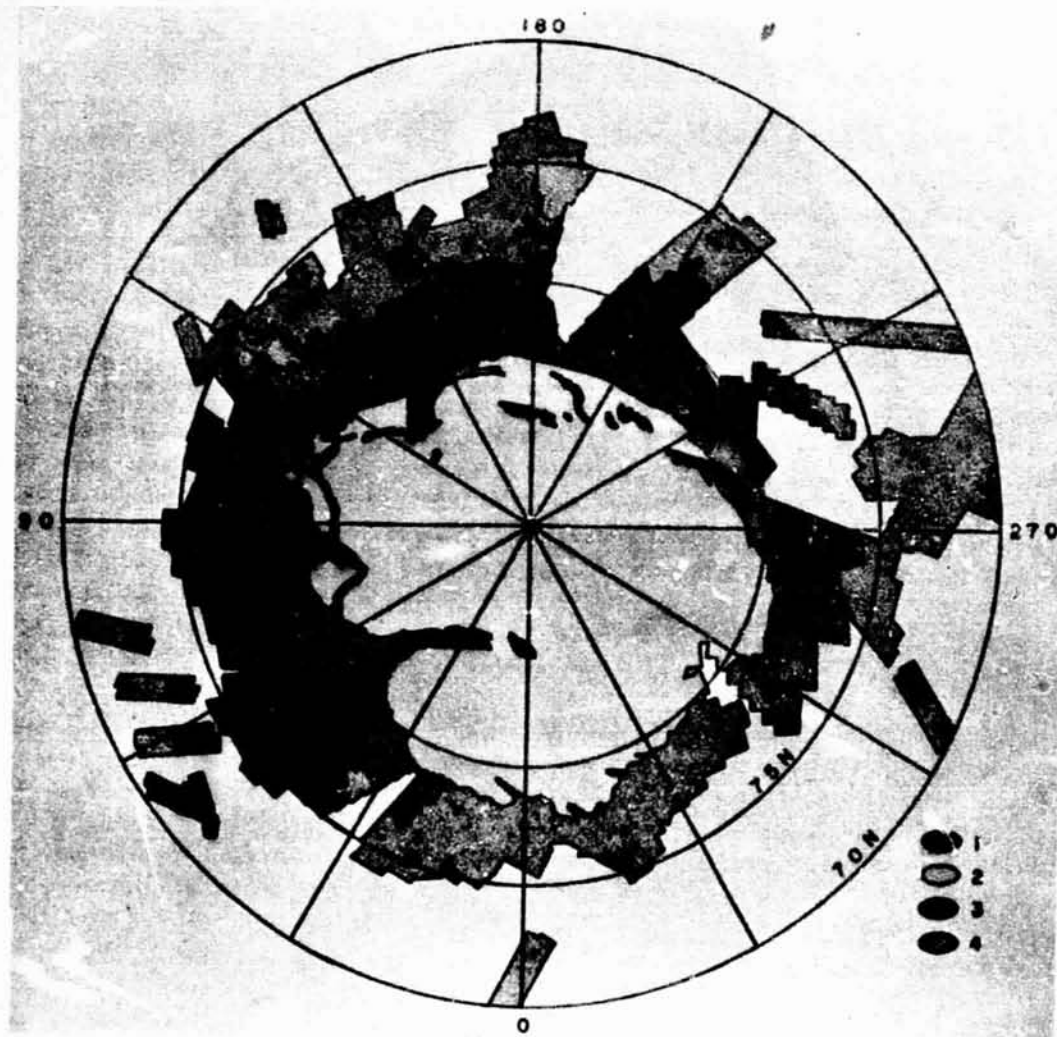
Figure 2: Stratigraphic map of the north polar region of Mars: (1) dunes, (2) layered deposits/perennial ice, (3) mantled plains, and (4) bulbous plains. Mantled plains include moderately- and heavily-mantled plains; bulbous plains include bulbous and lightly-mantled bulbous plains.

DESCRIPTION OF STRATIGRAPHIC UNITS

Bulbous Plains

The most heavily-cratered terrain in the north polar region is informally referred to as bulbous plains by this author. It is characterized by an abundance of small craters (<2 km diameter) relative to other north polar units (figure 9), by numerous debris-flow craters, and by a mottled, bulbous appearance (figure 3). The mottled, bulbous appearance is predominantly a result of bright material surrounding dark, highly irregular polygons, which are 3-8 km wide. Mottling is also due to concentrations of bright material inside and on the exterior rims of many craters. Within the same Viking Orbiter frame, the albedo of bulbous plains is generally intermediate between very dark dune deposits and bright mantled plains.

Mantled Plains

Mantled plains display a higher albedo than either bulbous plains or dune deposits, and has a crater population characterized by a deficiency of small craters relative to bulbous plains (figure 9) and by shallow craters commonly lacking visible ejecta (i.e. the appearance of burial). Mantled plains generally have a smooth appearance except for mesas and polygons in some areas (figure 4). Polygons seen in figure 4 are approximately the same width as those in bulbous plains (2-6 km) and are outlined by low-albedo markings or large troughs.

The gradational relationship of mantled plains to bulbous plains is seen in figure 5. Since craters and other surface features which are high in relief are the last features to be obscured with an increase in mantling, mantled plains are clearly shown to be overlying bulbous plains. The presence of a small bowl-shaped crater in the lower portion of the mosaic in figure 5 confirms that the obscuring of surface features in the lower portion is due to

surface mantling and not to cloud cover.

Dune Deposits

Dune deposits are characterized by a very low albedo relative to all other north polar units and commonly, though not always, by the presence of linear and arcuate patterns which have been interpreted as dunes (14). An excellent example of the relationship of dunes to mantled and bulbous plains is seen in figure 6.

Layered Deposits/ Perennial Ice Cap

Figure 7 shows an example of the layered deposits and the overlying perennial ice cap in the north polar region. The reader can refer to numerous other papers (8, 13, 14, 15) for detailed description and discussion of these units. The present paper will not examine these deposits in detail but will instead concentrate on stratigraphic units surrounding the north polar cap.
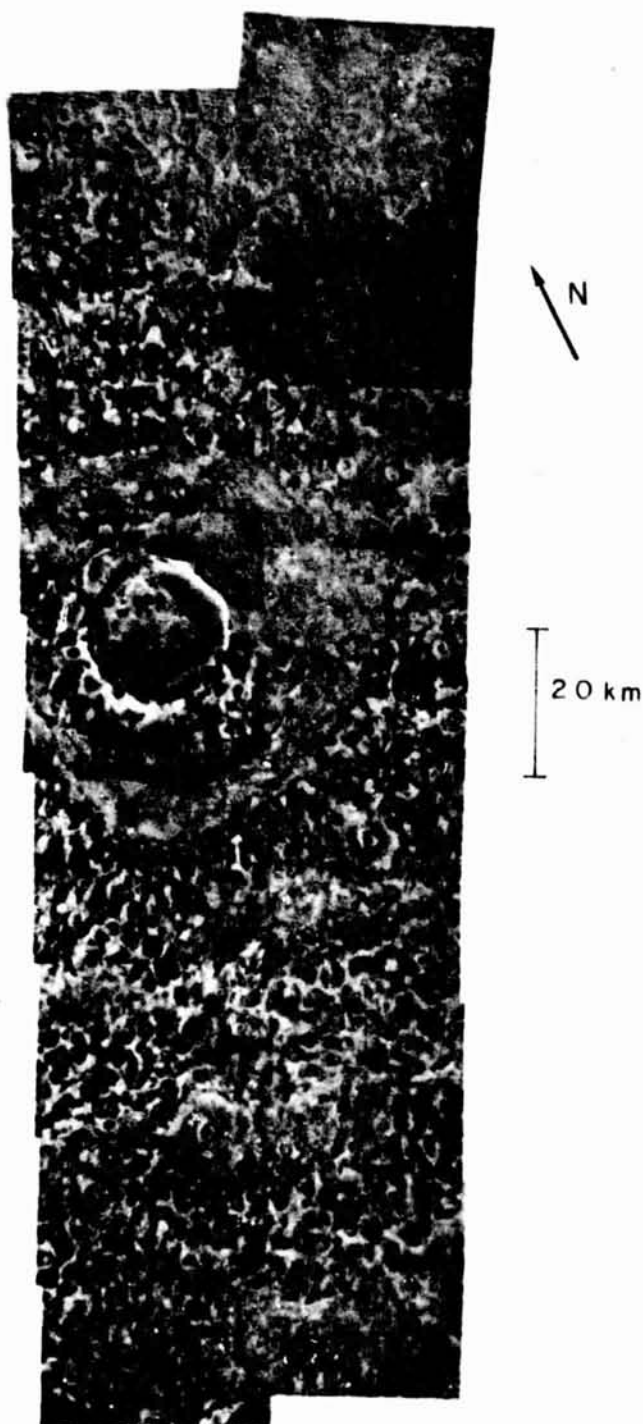
Figure 3: Type area for bulbous plains at 72°N, 290°W (Viking frames 538B01-538B16). Note the characteristic mottled, bulbous appearance resulting from bright material within and on the rims of craters and surrounding highly-irregular polygons.
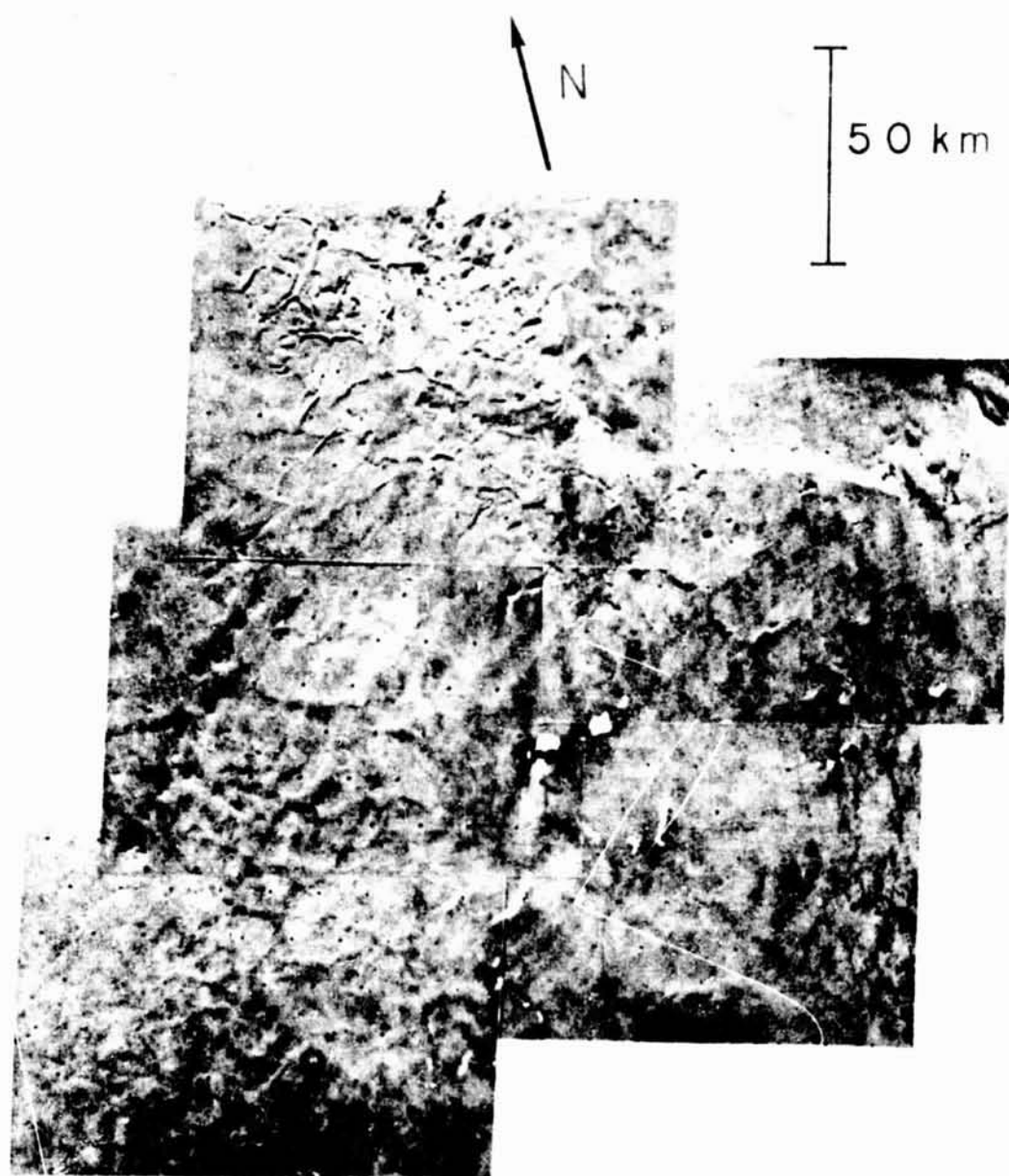
Figure 4: Type area for heavily-mantled plains, at the "mouth" of Borealis Chasma, 80°N, 65°W (Viking frames 70B31-70B35). Note polygons within mantled plains and layering in the scarp wall at the top of the mosaic (illumination is from the bottom right of the mosaic).

17
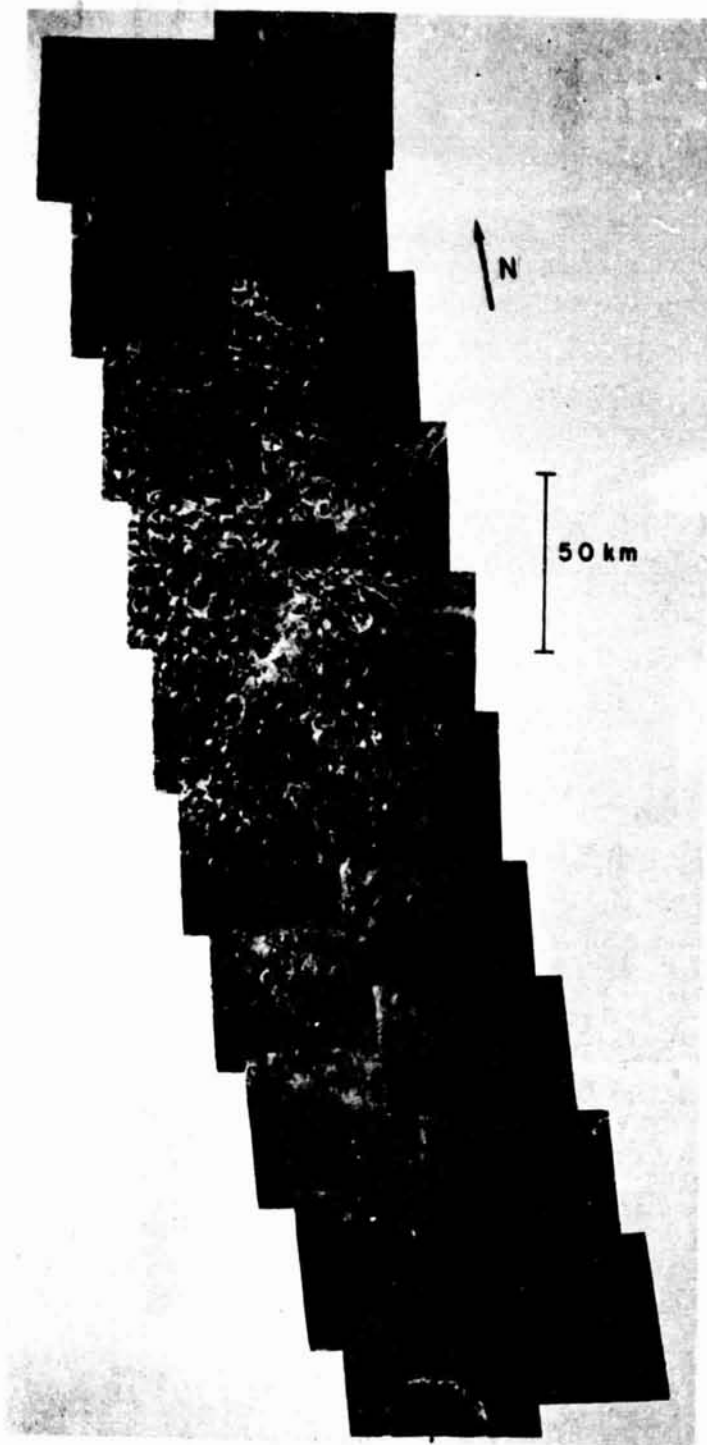
Figure 5: Viking Orbiter mosaic showing gradation of bulbous plains in the upper part of the mosaic to heavily-mantled plains in the lower part; at 70°N, 260°W (frames 576B10-576B20). The sharp appearance of the bowl-shaped crater (marked by arrow) indicates that the area is mantled rather than obscured by clouds. Also, note the two large "survivor" craters protruding through bulbous plains in the upper part of the mosaic.
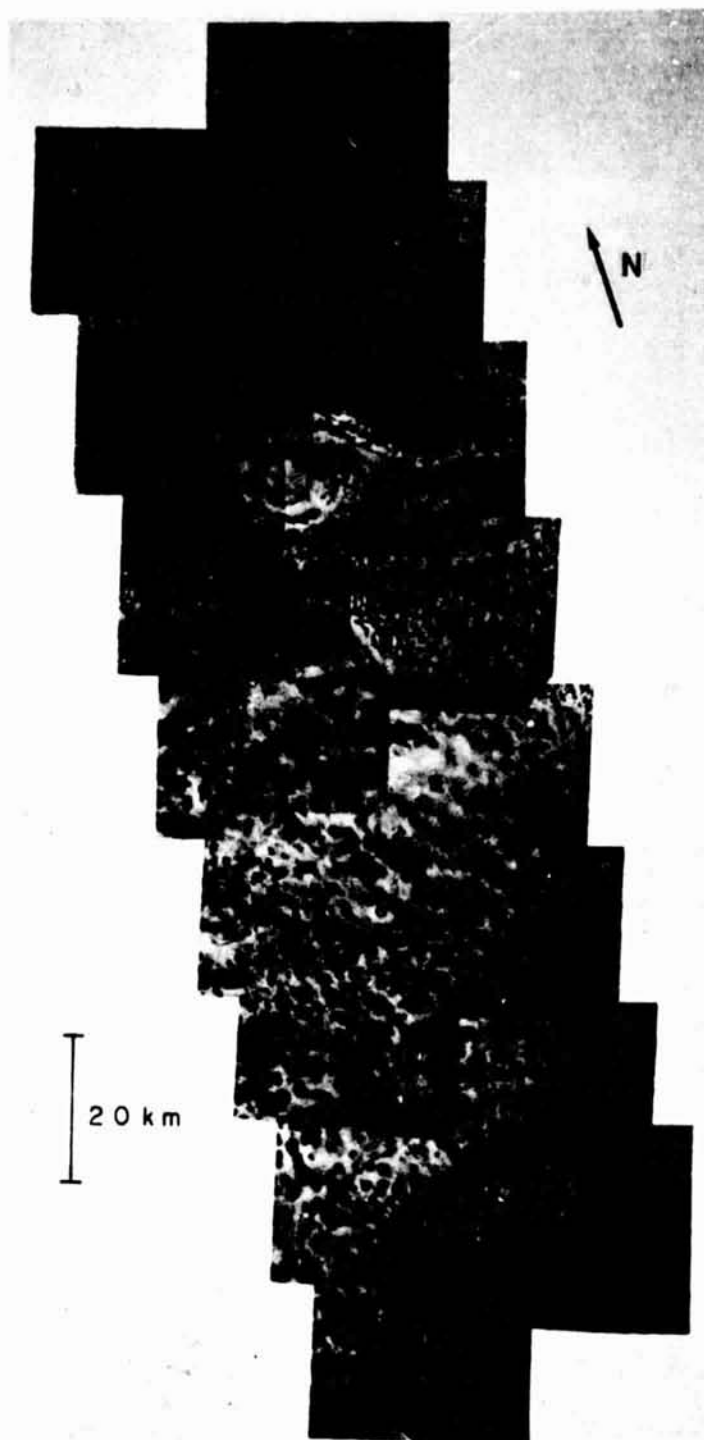
Figure 6: **Excellent** example of the relationships among bulbous plains, mantled plains, and dunes; at 72°N, 59°W (Viking frames 525B01-525B16). There is a relatively rapid gradation from bulbous plains near the bottom of the mosaic (south) to bright mantled plains and dark dunes in the north. Dunes in this mosaic are transverse and barchan dunes. Note the close correlation between the presence of dunes and the presence of mantled plains.

Figure 7: Viking Orbiter frame showing the bright perennial ice cap overlying layered deposits, which are exposed in the walls of troughs within the ice cap (frame 56B61).

INTERPRETATION AND DISTRIBUTION OF STRATIGRAPHIC UNITS

Bulbous and Mantled Plains

a. Interpretations from visual observations

Though certainly not the only possible interpretation, bulbous plains are interpreted here as having a volcanic origin. This is based primarily on its generally low albedo, though a history of near-surface igneous activity is also suggested by the presence of what appears to be an exposed dike (figure 8). Large "survivor" craters from the underlying older terrain can be seen protruding through bulbous plains in figure 8 and figure 5.

The highly-irregular polygons which characterize bulbous plains are somewhat different from polygons seen in lower latitudes. A belt of polygonal ground occurs between 40° and 50° N latitude, with typical polygons up to 20 km across (21). Polygons within bulbous ground are generally not larger than 8 km in diameter. Also, the patterned nature of bulbous plains appears to be more irregular than the polygonal appearance in the lower latitude belt, although this could be a result of the characteristic mottling of bulbous plains which tends to accent the irregular polygonal nature. As will be shown below, this mottling probably results from bright dust filling the low areas surrounding polygons and within craters. Thus, as the amount of dust-filling increases, polygon centers can be seen to stand out as highs.

The presence of the polygons in the lower latitudes of Mars has been attributed to contractive lava cooling or freeze-thaw ice wedging in a permafrost layer (21), although a scale problem exists when comparing Martian polygons to terrestrial analogs. Polygons formed by ice wedging or lava contraction on Earth are typically 100 m wide, whereas those in the 40°-50° N latitude belt of Mars are up to 20 km across (21). Although the highly irregular polygons within bulbous plains are generally not larger than 8 km,

this is still larger than terrestrial analogs. Still, the interpretation that polygonal ground on Mars may have formed by lava contraction or ice wedging is plausible. The unique occurrence of polygonal ground at latitudes greater than 40° N tends to favor the interpretation that polygonal ground on Mars results from ice wedging (21). However, since bulbous plains are confined to the northern latitudes, and may be volcanic, it is reasonable that either process might have formed its characteristic polygons.

As seen in figure 5, there is a gradation between mantled a ' ; ilbous plains, such that mantled plains range from lightly-mantled plains ' which some features of bulbous plains, such as a relative abundance of small craters and a mottled, polygonal appearance, are retained [reference Viking Orbiter frames 531B21-531B36], to moderately- and heavily-mantled plains, where bulbous characteristics are replaced by a relatively smooth, crater-deficient appearance [reference Viking mosaics 211-5573 (frames 71B61-71B62; 71B42-71B45) and 211-5562, respectively]. Due to this blanketing nature, mantled plains is interpreted as a deposit of wind blown dust covering bulbous plains in varying thicknesses.

Because of the difficulties involved in defining distinctive boundaries within highly gradational units, lightly-mantled plains are henceforth combined with bulbous plains to form a distinct mappable unit (figure 2). Thus, as presently defined, bulbous plains include all terrain which retain the characteristics of an abundance of small craters and a mottled, bulbous appearance. Likewise, moderately- and heavily-mantled plains which as will be discussed later could be arbitrarily separated on the basis of relative deficiences of small craters, are for convenience combined into a single map unit called mantled plains.

The presence of mesa-like landforms within mantled ground suggests that mantled plains have experienced a period of deflation. The origin of the

Figure 8a: Viking Orbiter mosaic showing what appears to be a linear dike and two "survivor" craters within lightly-mantled to moderately-mantled bulbous plains; at 70°N, 244°W (frames 505Bo1-505B13). Figures 8b and 8c are enlargements of these features and allow better discrimination of the underlying bulbous nature of the area.

Figure 8b: Enlargement of an ancient "survivor" crater seen in figure 8a,
allowing better discrimination of the underlying bulbous plains character-
istics, which are somewhat obscured by mantling.
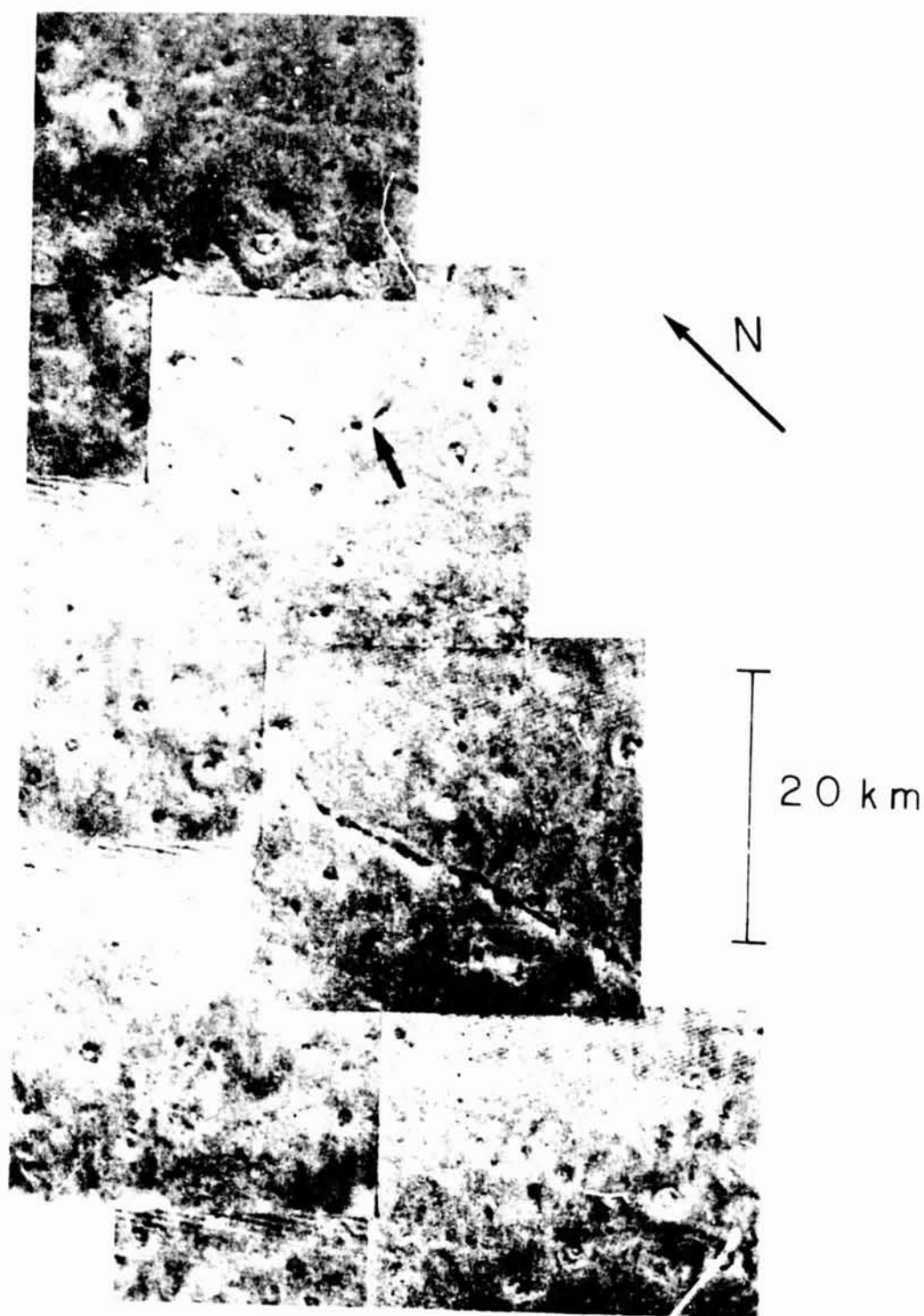
Figure 8c: Enlargement of a possible linear dike seen in figure 8a. Note that the length of the feature is greater than 20 km. The dike apparently protrudes through the mantling and the bulbous plains.

polygons within heavily-mantled plains is as poorly understood as the origin of the polygons which characterize bulbous plains. The similarity in size, however, suggests that either the process of formation is similar, or the polygons of mantled plains are controlled by underlying bulbous plains polygons.

b. Cumulative crater size-frequency distributions

Cumulative size-frequency distribution plots for small craters (< 10 km) on bulbous and mantled plains are presented in figure 9. The two plots for bulbous plains (figures 9a and 9b) represent the areas seen in figures 3 and 6, respectively. Clusters of similar-sized craters, like those seen in figure 3, result from secondary impact of ejecta from large impact events, and are generally not representative of the unit as a whole. Therefore, all craters which appeared to be associated with crater clusters were not included in the counts.

Both plots for bulbous plains display a power-law slope of about -2.0. A linear fit to the data gives a one-kilometer intercept "age" (22) of 4000 craters per 10^6 km^2.

An unrealistic decrease in the number of small craters counted in images can result from imagery degrading as crater diameters approach the resolution limits of the images. This results in a shallower slope, or a "rolling over," of the cumulative size-frequency distribution curve at small diameters. However, "rollover" due to resolution degradation for Viking Orbiter imagery occurs at 6 times the pixel resolution (23), or at 1.7×10^{-1} km for figure 9a. Since in figure 9a the break in slope occurs at 27 times the pixel resolution, or at 7.6×10^{-1} km, the slope of -0.7 for smaller crater diameters is probably a true feature of the crater population and not a resolution effect.

Crater size frequency distributions for mantled plains are seen in

figure 9c, with the plot for heavily-mantled plains representing the area at
the mouth of Borealis Chasma (figure 4). The plots for both moderately- and
heavily-mantled plains show a repetition of the shallow -0.7 slope observed
for smaller craters of bulbous plains. Moderately-mantled plains also display
a two-segment distribution curve, with a slope of -2.1 for crater diameters
larger than about 6 km. A slope of -2.1 is equivalent to the -2.0 to -2.2
slope values for large craters of bulbous plains.

A composite of figures 9a and 9c is seen in figure 9d. The curve
segments are for bulbous (curve A), moderately-mantled (curve B), and
heavily-mantled (curve C) plains. When adjusted for cumulative size-frequency
functions rather than differential size-frequency functions, the Jones and
Chapman model for crater obliteration (24) states that two segment curves,
such as A and B in figure 9d, represent a balance between a production
function,

$$\Psi(x) = \int_0^\infty c_d(x) \int_{T-t_e}^T c_t(t) \, dx \, dt \qquad [1]$$

and a cratering-obliteration equilibrium function,

$$\Psi(x)_e = [\, c_t(T) \, / \, o(T) \,] \int_D^\infty a(x) \, c_d(x) \, dx \qquad [2]$$

where x = the crater diameter, t_e = the retention age of a crater of a
given diameter, $c_t(T)$ = the time dependence of the cratering rate, $c_d(x)$ =
the diameter dependence of the cratering rate $(c_d(x) = D^{-k})$, $o(T)$ = the
obliteration rate, and $a(x)$ = the amount of obliteration needed to render a
crater indiscernable. Since the amount of obliteration, $a(x)$, needed to
remove a small crater is less than that needed for a larger crater, the
cumulative size-frequency plot for an obliterated (e.g. dust-mantled) surface

would show a shallow slope for small diameters, and a steep slope for larger diameters. Such is the case for curves in figure 9d. The repetition of -2.0 and -0.7 slopes for plots of both bulbous and mantled plains strongly suggests that the curves represent an equilibrium, or post-transient, cratering-obliteration process. Thus, using the Chapman-Jones model, -2.0 would define the slope of the production function, while the slope of -0.7 would represent a cratering-obliterat'on equilibrium function.

The repetition of the -0.7 equilibrium slope for all crater size-frequency distribution plots given above implies that the functions D^{-k} and $a(x)$ do not change from one area to another. Otherwise, the slopes would not be the same. Thus, making the reasonable assumption that the time-dependent cratering rate, $c_t(T)$, is also constant for all areas of concern, then the value of the equilibrium function, $\Psi_e(T)$, for a given diameter range, is dependent only on the obliteration rate, $o(t)$. Thus, the ratio of equilibrium frequencies, Ψ_e, for two such areas, would allow a relative obliteration rate, $o(t)$, to be calculated:

$$\frac{\Delta \Psi(x)_{e_1}}{\Delta \Psi(x)_{e_2}} = \frac{[\, c_t(T)_1 \,/\, o(T)_2 \,] \int_{D_a}^{D_b} a(x)_1 \, c_d(x)_1 \; dx}{[\, c_t(T)_2 \,/\, o(T)_2 \,] \int_{D_a}^{D_b} a(x)_2 \, c_d(x)_2 \; dx} \qquad [3].$$

For $c_t(T)_1 = c_t(T)_2$, $a(x)_1 = a(x)_2$, and $c_d(x)_1 = c_d(x)_2$:

$$\frac{\Delta \Psi(x)_{e_1}}{\Delta \Psi(x)_{e_2}} = \frac{o(T)_2}{o(T)_1} \qquad \qquad [4]$$

From figure 9d, the relative obliteration rates for bulbous : moderately-mantled : heavily-mantled plains are calculated as 1:9:88.

The change of slope of about 1 between crater-production and obliteration-equilibrium functions of the north polar units is consistent with the simple dust-filling model of Chapman (25). This supports this author's interpretation that mantled plains are deposits of wind-blown dust covering bulbous ground in varying thicknesses. The break in slope between crater-production and obliteration-equilibrium functions is a result of the presence of "survivor craters" which have not been obscured by the obliteration process (22). Thus, if dust mantling is the only obliterating process acting, the diameter at which the function slope changes (i.e. the "kink point") should be an indication of the average thickness of the dust mantle. Based on crater data for the Martian surface, Cintala and Mouginis Mark (26) empirically derived that the crater depth = $0.104 \times$ diameter$^{0.962}$ for craters less than 12.3 km in diameter. By substituting the kink-point diameter for moderately-mantled plains into the equation, the thickness of the dust layer comprising moderately-mantled plains is calculated to be about 600 m. Since the crater-function kink for heavily-mantled plains does not occur within the range of diameters plotted, the thickness of dust deposited in this region is, at least, the depth of the largest crater measured, or 770 m. These values are somewhat higher than the 200 m maximum predicted by Squyres (15).

The data points seen on the composite plot (figure 9d) are not data from north polar units, but are instead the data from Neukum and Wise (22) for a cratered plains unit at Tempe Plateau (30°N, 90°W). The excellent correlation between their data and the composite plot for bulbous and moderately-mantled plains suggests first that the crater function for bulbous plains may follow the moderately-mantled plains curve in the region of diameters greater than 5 km. Since only smaller craters would be buried by an obliteration episode, this is a reasonable assumption if moderately-mantled plains result from obliteration of bulbous plains. However, such a theory should certainly be
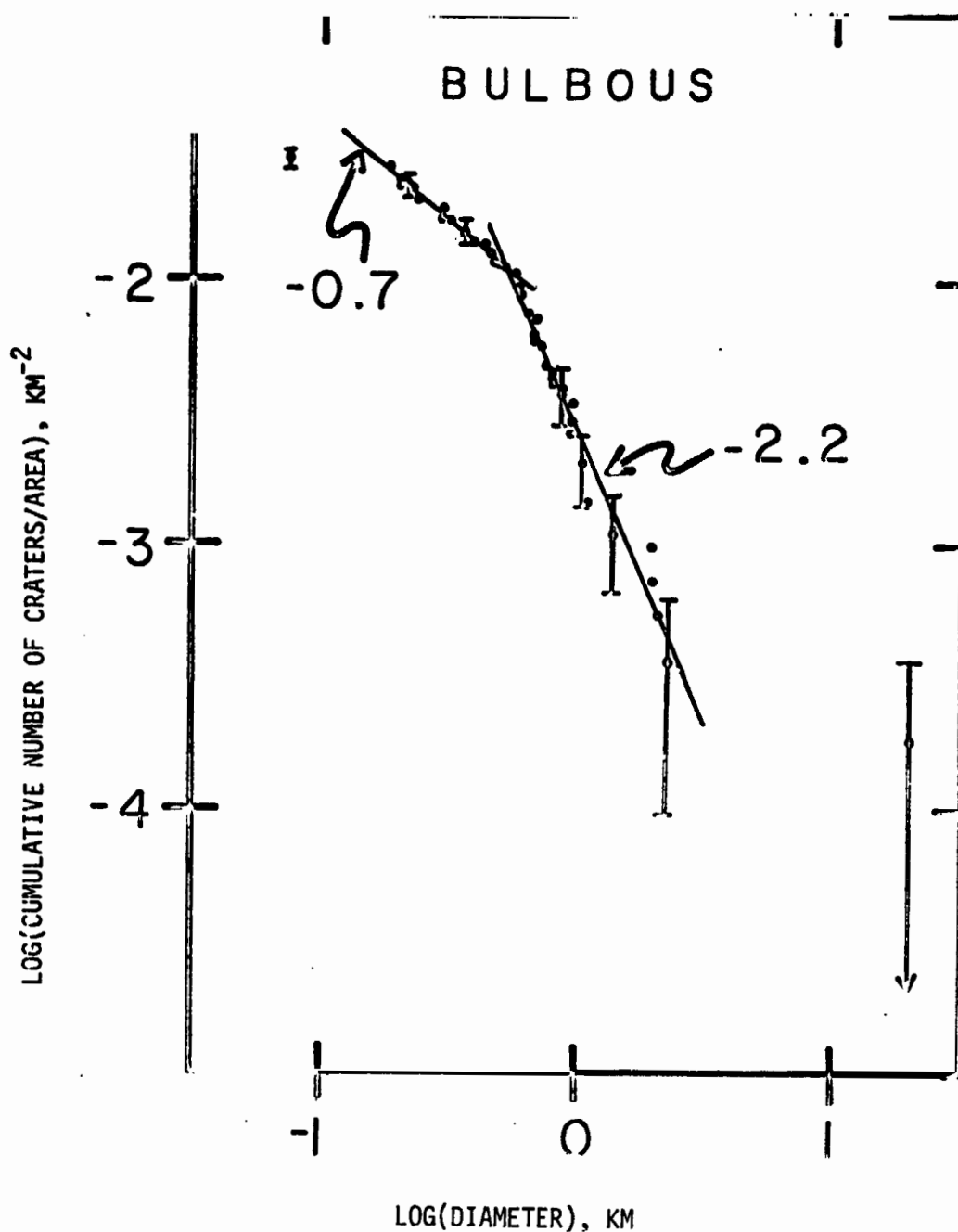
Figure 9a: Cumulative size-frequency distribution plot for small craters on bulbous plains. Area represented is from the bulbous plains type area seen in figure 3. N = 156 craters; total area = 5,419.1 km². Error bars signify one standard deviation confidence intervals and equal $\pm \sqrt{n}$ for the nth crater.
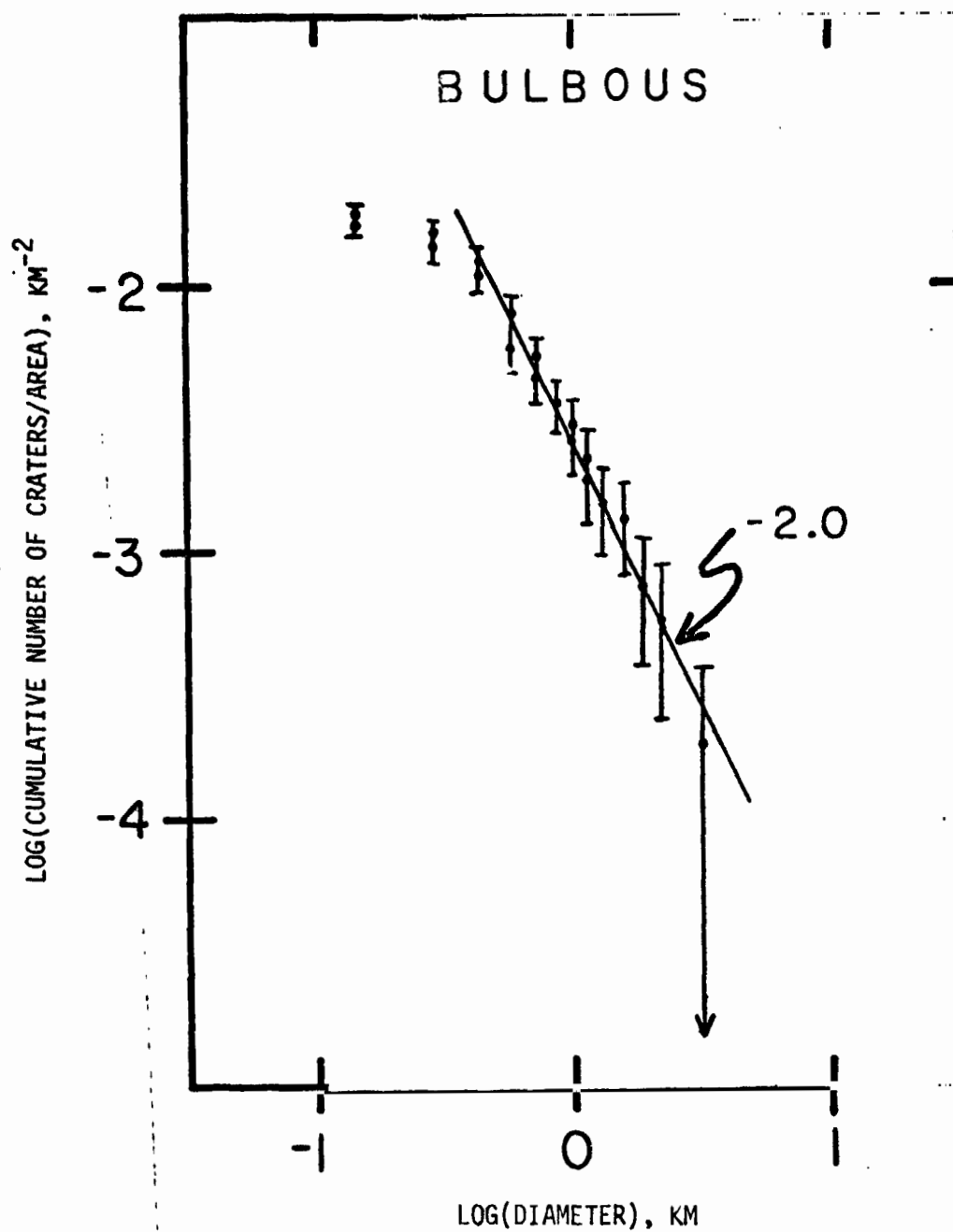
Figure 9b: Cumulative size-frequency distribution plot for small (< 4 km) craters on bulbous plains, representing the area seen in figure 6. N = 97 craters; total area = 5,400.7 km^2.
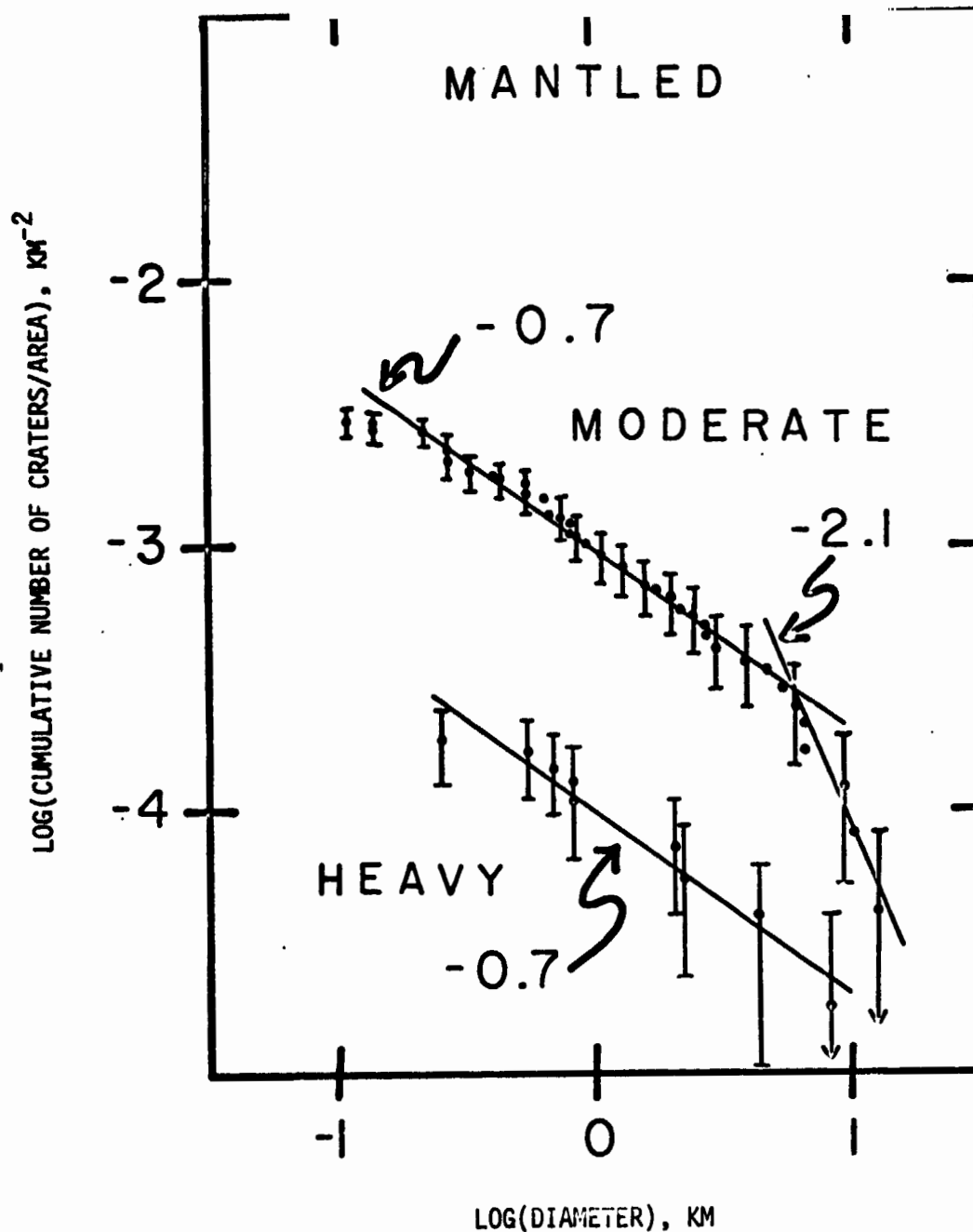
Figure 9c: Cumulative size-frequency distribution plots for small (⊕ 13 km) craters on mantled plains. The heavily-mantled plains plot represents the type area at Borealis Chasma seen in figure 4. N = 9 craters; total area = 55,120.6 km². The curve for moderately-mantled plains is for the area at 76°N, 90°W (Viking frames 70B04, 71B61-71B64). N = 71 craters; total area = 24,344.6 km².
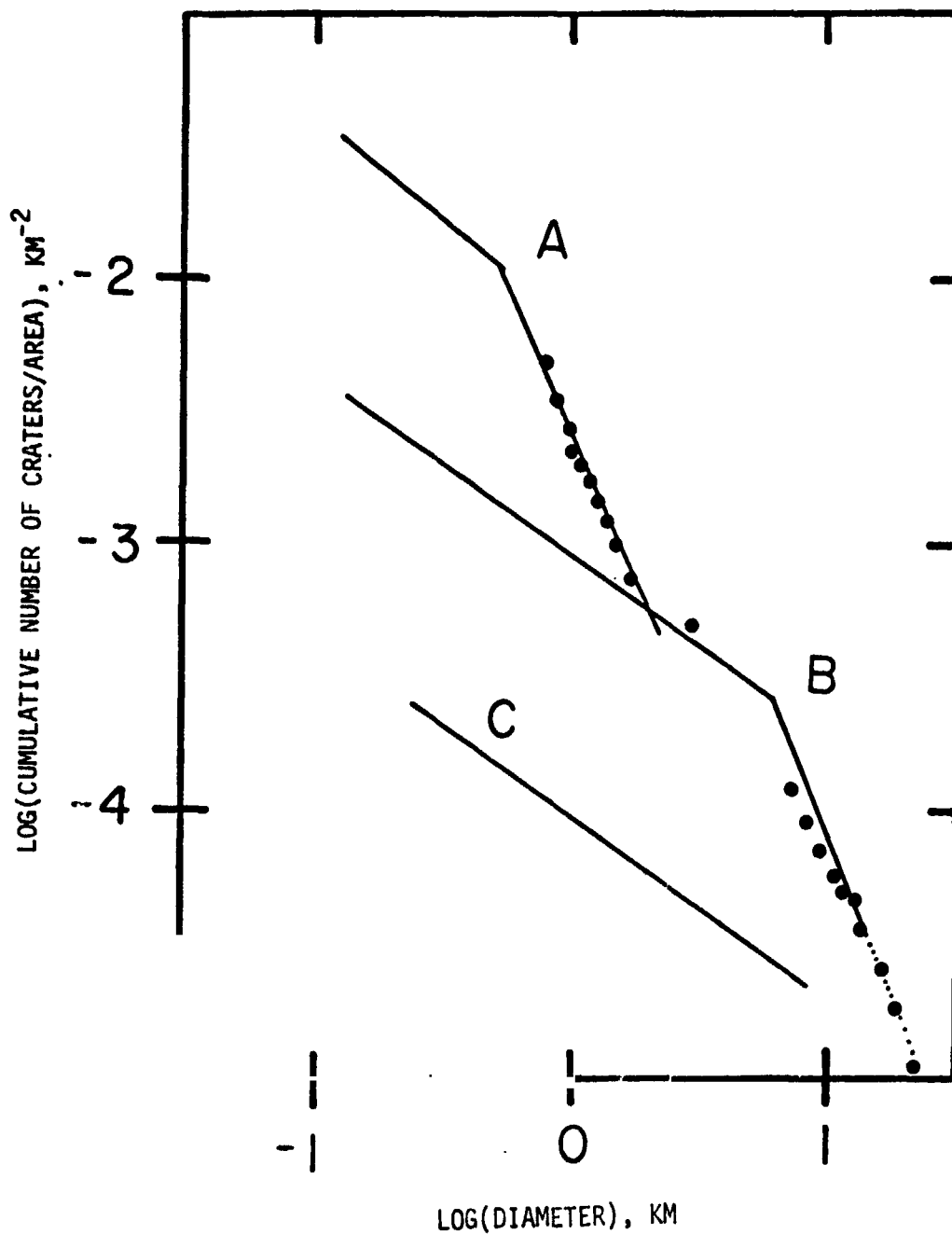
Figure 9d: Composite of cumulative crater size-frequency distribution curves seen in figures 9a and 9c. Curve A - bulbous plains; curve B - moderately-mantled plains; curve C - heavily-mantled plains. Data points are from Neukum and Wise (22) for a cratered plains unit at Tempe Plateau, 30°N, 90°W.

tested by plotting the crater distribution curve for greater than 5 km craters
on bulbous plains.

Of more importance is that the correlation of the bulbous plains
crater plot with that of the cratered plains unit at Tempe Plateau, places
bulbous plains within the Martian global stratigraphic sequence as one of the
relatively old cratered plains units. According to the time scale of
Neukum and Wise (22), bulbous plains has an "absolute" age of 3.8 b.y. (note:
according to the same scale, the oldest cratered plains unit, Lunae Planum,
is 3.9 b.y.).

Dune Deposits

Dunes in the north polar region of Mars are predominantly transverse and
barchan dunes, although some longitudinal dunes are also present. They are
similar in size to megadunes (draa) found in the Sahara, Arabia, and the
Algodones dune fields on Earth (36).

As suggested below, dune deposits might also occur as "sheet-sand"
deposits. Figures 1 and 2 show the stratigraphic map and a Mariner 9 mosaic
of the north polar region of Mars. A visual comparison between the strati-
graphic map and the Mariner 9 image between 30° - 290° W longitude confirms
that the dark circumpolar band seen in the mosaic correlates well with the
presence of dunes. However, in the region 290°-0°-30° W longitude, the
dark band extends into much of the area mapped as bulbous plains, whereas
other areas of bulbous plains, including the type area, are not as dark.
Though this region was often cloudy during much of the Viking Orbiter imagery
sequences, some relatively clear images (e.g. 531B21 - 531B36) confirm the
duneless, bulbous nature of the area. The presence of the low-albedo band
in duneless terrain suggests either a very thin "sheet-sand" deposit of dark
dune material overlying much of the most northern exposures of bulbous plains,

or that the albedo of bulbous plains in other areas is more influenced by a thin mantling of bright dust. Notice that even the type area for bulbous plains appears to have dust in many depressions (figure 3).

Actual dunes are generally confined to mantled regions, as illustrated in figure 6 and the stratigraphic map in figure 2. If dune deposits overlie bulbous plains, they occur predominantly as "sheet sand" deposits rather than dunes. This suggests that, unlike bulbous plains, mantled plains provide the proper substratum for the accumulation of dunes. Mantling probably creates a smooth, crater-deficient surface which might favor dune formation.

An observed eastward gradation from densely-spaced to more dispersed dunes provides valuable information for determining the source of the circum-polar dune deposits. Fields in the region of 130°-270° W longitude are exten-sive, uninterrupted fields with distinct boundaries and consisting of transverse dunes with very narrow interdune areas (figure 10, and Viking Orbiter Mosaics 211-5269 (rev.61), 211-5272 (revs. 60,61), 211-5431 (revs. 62,63), and 211-5583 (rev. 72)). Dunes within the 30°-130° W longitude region occur in more dispersed fields and are generally transverse and barchan dunes with wide, bare interdune areas (figure 11 and Viking Orbiter Mosaics 211-5269 (rev. 59), and 211-5562 (revs. 50,69)). Between 30°-0°-270° W longitude, dune deposits are predominantly in the form of very isolated dunes, or possibly as sheet sands. The overall view is one of counterclockwise gradation from dense transverse dunes in the region between 270° and 150° W longitude to more highly dispersed transverse and barchan dunes and eventually to possible sheet sands and isolated dunes. Although the presence of mantling appears to be required for dune formation, the degree of mantling does not appear to control the morphology of the dune fields. On Earth, transitions from trans-verse to barchan dunes and from narrow to wide interdune areas are generally related to a decrease in the supply of dune material (27). This relationship

is typically encountered as one moves progressively away from the source of sediment. Thus, the situation observed in the north polar region may be one of a counterclockwise thinning of the supply away from the source.

Layered Deposits

The layered deposits are probably a facies of mantled plains in which wind-blown dust is deposited onto the perennial ice cap rather than directly onto the ground (15). Although it is not clearly understood which changes in Mars' orbital parameters most affect the eventual growth and decay of the perennial ice caps (3), the extent of layered deposits at the poles probably indicates the maximum extent of the perennial ice caps in the past.

Relationships of units at Borealis Chasma may illustrate an interfingering of mantled plains and layered deposits. Layering can be seen in the scarp which overlies mantled plains at the "mouth" of Borealis Chasma (figure 4). However, the surface of much of Borealis Chasma does not display the laminations within minor topography as is typical of north polar layered deposits. The surface of Borealis Chasma instead has the appearance of mantled plains, suggesting a transition from mantled plains to layered deposits and back to mantled plains. Such a transition is not unreasonable since the extent of the perennial ice cap is expected to fluctuate with time.

Comparison with Previous Research

The north polar stratigraphy presented in this paper has been compared to the stratigraphy proposed by Soderblom et. al. (11), and that of Squyres (15). Although the preliminary stratigraphic map of Soderblom et. al. has been greatly altered, their basic stratigraphic sequence for the north polar region has not changed drastically. Bulbous plains are certainly a sub-unit of the "mottled cratered plains" unit which includes a large portion of the northern hemisphere. However, bulbous plains with their characteristic highly-

irregular polygonal appearance are probably confined to the northern portion of the mottled cratered plains. Mantled plains are equivalent to the debris mantle and etch-pitted plains in the stratigraphic sequence of Soderblom et. al., whereas dune deposits replace the rippled plains.

Although the stratigraphic sequence proposed in this paper agrees in theory with that proposed by Squyres (15, 28), there are very serious discrepancies in the defining and mapping of the cratered plains and mantled units. The previous author's type locale and only exposure of his underlying "cratered plains" unit is at the mouth of Borealis Chasma. This same area, seen in figure 4 and represented by the crater plot for heavily-mantled plains in figures 9c and 9d, is the present author's most heavily-mantled unit in the north polar region. Both the imagery and the crater size-frequency distribution data for this area show an obvious deficiency of craters relative to moderately-mantled and bulbous plains. Also, as discussed earlier, the shallow slope of -0.7 confirms that the unit is a highly-obliterated surface, probably resulting from a dust mantling which may be at least about 700 m thick. Units represented by curves A and B in figure 9d are one to two orders of magnitude more cratered than the "cratered plains" unit of Squyres. Both units represented by curves A and B have been mapped by the previous author as a debris mantle which formed by dust obliteration of craters on the "cratered plains" unit represented by curve C. Such an interpretation of these units is obviously not consistent with the crater size-frequency distribution function for these areas.

Figure 10: Viking Orbiter frame showing circumpolar dune field typical of those within the area between 130° and 270° W longitude (frame 59B35). Dunes in this region are predominantly uninterrupted and closely-spaced transverse dunes. Also note the crisscross pattern of the northwestern dunes indicating modification from secondary winds sweeping off the cap.

38
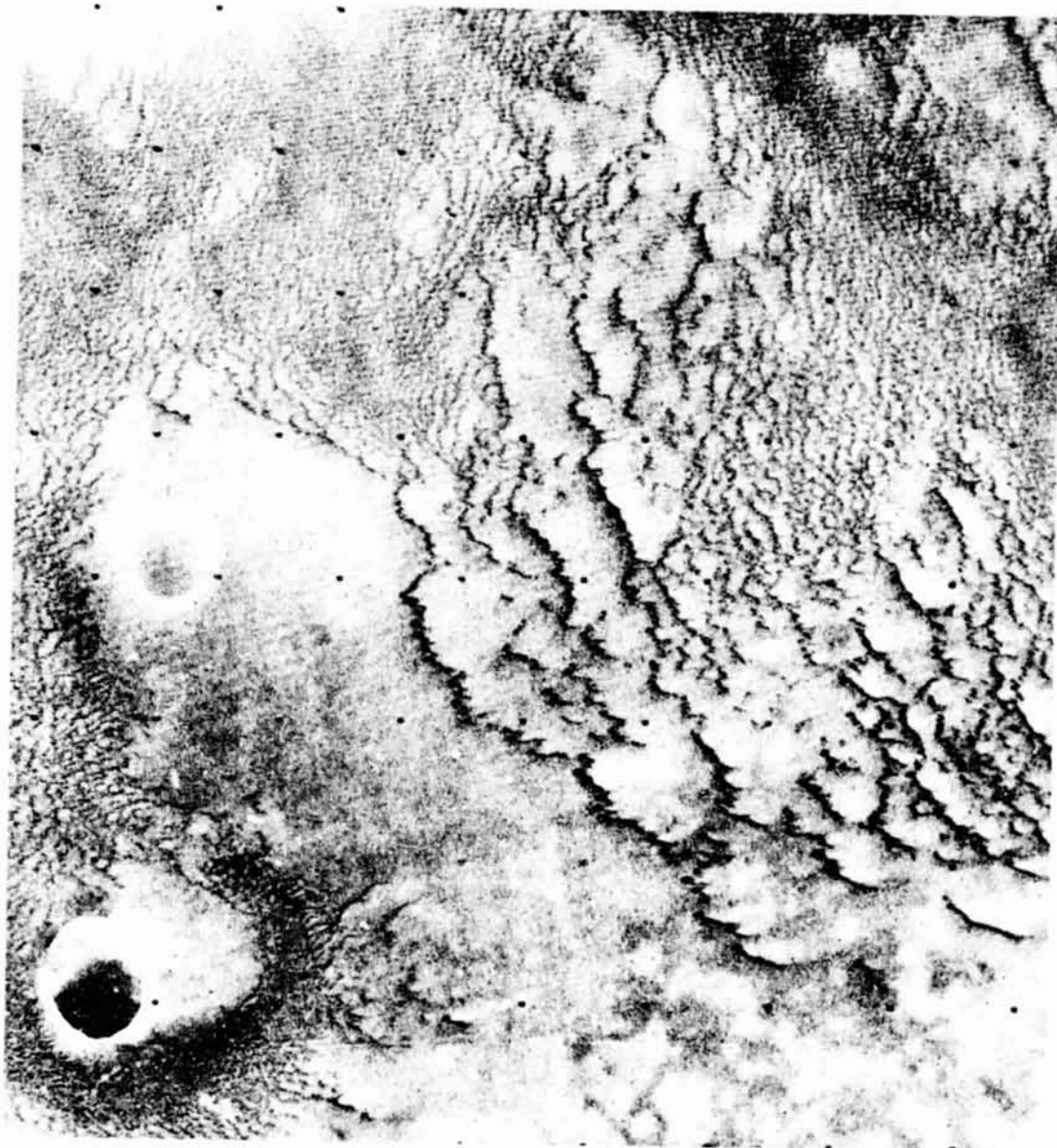
Figure 11: Typical dune field within the north polar region between 30°
and 130° W longitude (Viking frame 71B64). These dunes are barchan and
transverse dunes with wide interdune areas, indicating a sparseness of
supply.

Numerous investigators (29, 30, 31), including the present author (this paper), have independently inferred near-surface wind directions within the north polar region of Mars, on the basis of dune orientations. Figure 12 shows dune orientations mapped from orthographic images which minimize distortions resulting from "oblique viewing" of the spacecraft. The map presents data in the form of orientations of arcuate (barchan) dunes and the trend of linear (transverse and longitudinal) dunes. The crisscross pattern of the dunes between 150° and 210° W longitude can be seen in figure 10.

Caution must be exercised when interpreting wind directions based on dune orientations derived from Viking Orbiter images. In such cases, barchan forms provide the most reliable indicators of near-surface wind orientations. Transverse and longitudinal dunes in the circumpolar images generally only allow determination of a wind trend rather than a wind direction. Thus, interpretations based on transverse and longitudinal dunes must rely on indirect evidence, such as wind streaks or directions based on nearby barchan dunes. Tsoar et. al. (31) have attempted to determine absolute wind dir-directions based on the asymmetry of transverse dunes. However, it is again cautioned that the resolution of Viking north polar images may not allow reliable separation of true dune slope asymmetry from illusory effects due to shadows or oblique viewing.

In figure 13 is the present author's interpretation of wind directions based primarily on orientations shown in figure 12. Interpretations of wind directions for the transverse dune fields between 120° and 240° W longitude relied on the assumption of a continuity of wind flow relative to barchan dunes which occur at the edge of the field. Wind directions in figure 13

indicate a predominantly counterclockwise flow of dune-driving winds around the ice cap along with dune modifying winds which spiral clockwise off of the ice cap, possibly during a change in season. Such an interpretation of wind directions is consistent with north polar wind circulation patterns derived from streak orientations (29), from lee cloud orientations (32; R.G. French, personal communication, 9/25/79), and from other interpretations based on dune orientations (29, 30, 31). Leach (30) attributes the clockwise pattern to the influence of Coriolis force acting on katabatic winds spiralling off the ice cap.

Thus, data derived from dune, wind streak, and lee cloud orientations indicate a polar atmospheric circulation pattern consisting of winds travelling around the ice cap in a counterclockwise direction, modified by katabatic winds spiralling clockwise off of the ice cap. Such a pattern is similar to the wind circulation around the Antarctic ice cap on Earth (30).
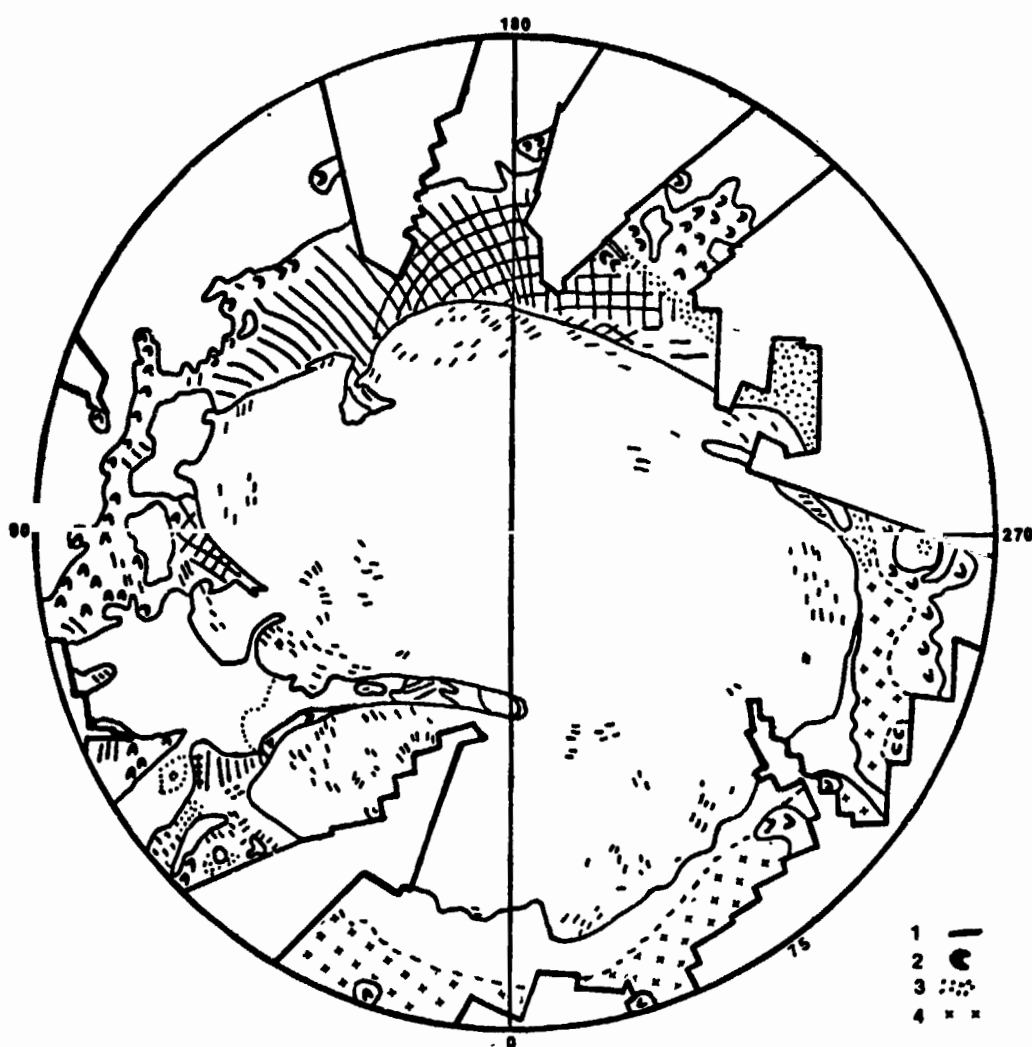
Figure 12: Dune trends within the north polar region of Mars. (1) linear
trends within dune fields, and grooves in ice, (2) direction of arcuate forms
in dunes (asymmetry of symbols corresponds to asymmetry observed), (3) complex
dunes with no distinct linear or arcuate patterns, and (4) possible sheet sand
deposits. Symbols signify general trends of dunes rather than individual dunes.
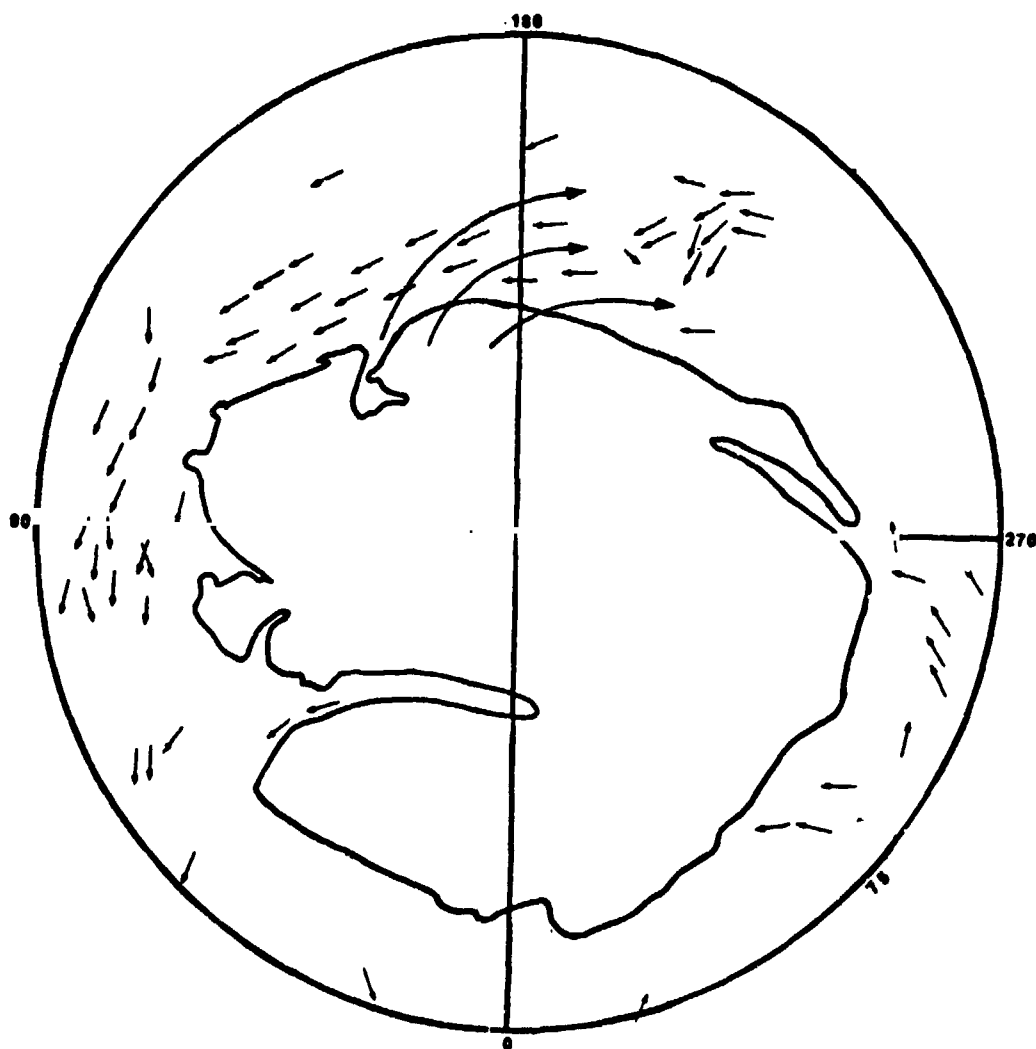
Figure 13: Near-surface wind directions based primarily on orientations seen
in figure 12. There is a predominant counterclockwise direction of flow around
the ice cap, with modification by winds spiralling off the cap.

IMPLICATIONS FOR THE SOURCE OF CIRCUMPOLAR DUNE MATERIAL

As discussed earlier, the gradation of extensive, uninterrupted transverse dune fields to scant fields with widely spaced transverse and barchan dunes implies a general decrease in the supply of dune material as one moves eastwardly (or counterclockwise) away from the area between 270° and 180° W longitude. Circumpolar winds were found to flow predominantly counterclockwise, suggesting a general thinning of dune deposits in a downwind direction. This, combined with the presence of extensive exposures of bulbous plains upwind of extensive dune fields, may indicate that dune material is stripped from bulbous plains and deposited on mantled regions.

Such a conclusion might be further supported if one considers the dark circumpolar band extended into duneless bulbous plains areas. Two possible interpretations were suggested earlier to account for this, one being that a very thin sheet sand deposit of dark dune material blankets bulbous plains in this area, and the other suggesting that bulbous plains in this area are more completely stripped of a thin bright dust layer than bulbous plains in other areas. The first interpretation is consistent with dune material being continually derived from bulbous plains only to be slowly stripped from the region and deposited onto mantled plains downwind. If the second interpretation were true it would lend very strong support to the suggestion that bulbous plains are the source of the dune deposits. Not only would it provide evidence that this possible source area is significantly stripped, but more importantly it would indicate that bulbous plains and dune deposits have the same low albedo.

CONCLUSION

The stratigraphic sequence of the north polar region of Mars can be separated into four distinct informal units: (a) bulbous plains, (b) mantled plains, (c) dune deposits, and (d) layered deposits/perennial ice.

Bulbous plains is a relatively old "mottled" cratered plains unit equivalent in crater-distribution age to the cratered plains unit at Tempe Plateau (90°W, 30°N). According to the time scale of Neukum and Wise, the "absolute age" of bulbous plains is 3.8 b.y.. Due to its relatively low albedo and because of near-surface volcanics suggested by the presence of what appears to be a dike, bulbous plains are interpreted as having a volcanic origin. Polygons within bulbous plains are 3-8 km and may have formed by contractive cooling of lava or freeze-thaw ice wedging within a permafrost layer.

Mantled plains are interpreted as wind-blown dust deposits covering bulbous plains in varying thicknesses. A deficiency of small craters seen in crater size-frequency distribution functions for bulbous and mantled plains supports the interpretation that mantled plains formed by obliteration of bulbous plains, while a change of slope of about 1 between crater-production and obliteration-equilibrium functions for north polar units is consistent with obliteration by dust-filling. The relative surface-obliteration rates are 1:9:88 for bulbous, moderately-mantled, and heavily-mantled plains, respectively.

Previous stratigraphic mapping proposed by Squyres for the north polar region of Mars is inconsistent with interpretations based on crater size-frequency distribution data. Such evidence strongly supports that his "cratered plains" unit at the mouth of Borealis Chasma is instead a heavily-mantled plains, whereas many areas mapped by the previous author as "debris

mantle" are instead cratered plains.

Layered deposits probably represent a facies of mantled plains in which dust is deposited onto the perennial ice cap rather than directly onto the ground. Thus, the extent of the layered deposits at the north and south poles may indicate the maximum extent of the perennial ice caps in the past. A possible interfingering of layered deposits and mantled plains can be seen at the mouth of Borealis Chasma.

Dunes in the north polar region of Mars have a very low albedo and occur as transverse, barchan, and to a minor extent, as longitudinal dunes. Actual dunes are generally confined to mantled plains, suggesting that mantling provides a proper substratum for dune formation. The extension of the dark circumpolar band into duneless areas mapped as bulbous plains suggests that thin sheet sand deposits overlie bulbous plains in this area or that the most northern exposures of bulbous plains have been more effectively stripped of bright dust than bulbous plains in other areas. If the latter interpretation is true, it indicates that the albedo of bulbous plains is similar to the albedo of the dunes. The distribution of dune forms and dune field styles reveals thinning of the supply of dune material in an eastward direction away from the area between 270° and 180° W longitude.

As determined from dune orientations, near-surface north polar winds consist of a counterclockwise flow around the ice cap modified by katabatic winds spiralling clockwise off the cap. This is analogous to the atmospheric circulation pattern around the Antarctic ice cap on Earth.

The results above suggest a general thinning of the supply of dune material downwind of the area between 270° and 180° W longitude. Immediately upwind of this area are extensive exposures of bulbous plains. Thus, the author suggests that dune material is being stripped from bulbous plains and is accumulating as dunes downwind on mantled plains.

BIBLIOGRAPHY

(1) Slipher, E.C. (1962) The Photographic Story of Mars, Sky Publishing
       Corporation, Massachusetts.

(2) Hartmann, W.K., and O. Raper (1974) The New Mars: The Discoveries of
       Mariner 9, NASA SP-337, 108-122.

(3) Mutch, T.A., R.E. Arvidson, J.W. Head III, K.L. Jones, R.S. Saunders
       (1976) The Geology of Mars, Princeton University Press, New Jersey,
       17-18, 86-91, 250-254.

(4) Murray, B.C., and M.C. Malin (1973) Polar wandering on Mars?, Science,
       179, 997-1000.

(5) Cutts, J.A. (1973) Wind erosion in the Martian polar regions, J. Geophys.
       Res., 78, 42211-4221.

(6) Cutts, J.A., and W.L. Michalsky (1975) Mars: A new type of landscape
       feature in the south polar region, Final Report, contract 954189,
       Jet Propulsion Lab., Pasadena, CA.

(7) Murray, B.C., L.A. Soderblom, J.A. Cutts, R.P. Sharp, D.J. Milton, and
       R.B. Leighton (1972) A Geological framework for the south polar
       region of Mars, Icarus, 17, 328-345.

(8) Sharp, R.P. (1973) Mars: south polar pits and etched terrain, J.
       Geophys. Res, 78, 4222-4230.

(9) Cutts, J.A. (1973) Nature and origin of layered deposits in the
       Martian polar regions, J. Geophys. Res., 78, 4231-4249.

(10) Sagan, C., J. Veverka, P. Fox, R. Dubisch, R. French, P. Gierasch,
       L. Quam, J. Lederberg, E. Levinthal, R. Tucker, B. Eross, and
       J.B. Pollack (1973) Variable features on Mars 2, Mariner 9 global
       results, J. Geophys. Res., 78, 4163-4196.

(11) Soderblom, L.A., M.C. Malin, J.A. Cutts, and B.C. Murray (1973) Mariner
       9 observations of the surface of Mars in the north polar region,
       J. Geophys. Res., 78, 4197-4210.

(12) Kieffer, H.H. T.Z. Martin, A.R. Peterfreund, B.M. Jakosky, E.D. Miner,
       and F.D. Palluconi (1977) Thermal and albedo mapping of Mars
       during Viking primary msision, J. Geophys. Res., 82, 4249-4291.

(13) Howard, A.D. (1978) Origin of the stepped topography of the Martian
       poles, Icarus, 34, 581-599.

(14) Cutts, J.A., K.R. Blasius, G.A. Briggs, M.H. Carr, R. Greeley, H. Masursky
       (1976) North polar region of Mars: imaging results from Viking 2,
       Science, 194, 1329-1337.

(15) Squyres, S.W. (1979) The geology of the Martian north polar region, Unpublished report, Cornell University.

(16) Sagan, C., D. Pieri, P. Fox, R.E. Arvidson, and E.A. Guinness (1977) Particle motion on Mars inferred from the Viking Lander cameras, J. Geophys. Res., 82, 4430-4438.

(17) Pollack, J.B., D. Colburn, R. Kahn, J. Hunter, W. Van Camp, C.E. Carlston, and M.R. Wolf, (1977) Properties of aerosols in the Martian atmosphere, as inferred from Viking Lander imaging data, J. Geophys. Res., 82, 4479-4496.

(18) Haberle, R.M., C.B. Leovy, J.B. Pollack (1979) A numerical model of the Martian polar cap winds, (in press).

(19) French, R.G., and P.J. Gierasch (1979) The Martian polar vortex: seasonal variation and observations of eolian features, J. Geophys. Res., 84, 4634-4642.

(20) Greeley, R. and R. Leach (1978) A preliminary assessment of the effects of electrostatics on aeolian processes, Reports of Planetary Geology Program 1977-1978, NASA TM 79729, 236-237.

(21) Carr, M.H. and G.G. Schaber (1977) Martian permafrost features, J. Geophys. Res., 82, 4039-4054.

(22) Neukum, G., and D.U. Wise (1976) Mars: A standard crater size-frequency distribution curve and a possible new time scale, Science, 194, 1381.

(23) Masursky, H., J.M. Boyce, A.L. Dial, G.G. Schaber, and M.E. Strobell (1977) Classification and time of formation of Martian channels based on Viking Data, J. Geophys. Res., 82, 4016-4038.

(24) Chapman, C.R., and K.L. Jones (1977) Cratering and obliteration history of Mars, Ann. Rev. Earth Planet. Sci., 5, 515-540.

(25) Opik, E.J. (1975) Mariner IV and craters on Mars, Irish Astron. Jour., 7, 92-104.

(26) Cintala, M.J., and P.J. Mouginis-Mark (1979) New depth/diameter data for fresh Martian craters and some interplanetary comparisons (Abstract), Reports of Planetary Geology Program, 1978-1979, NASA TM 80339, 182-184.

(27) Glennie, K.W. (1970) Desert Sedimentary Environments; Developments in Sedimentology 14, Elsevier Publishing Co., New York, Chap. 6.

(28) Squyres, S.W. (1979) The evolution of dust deposits in the Martian north polar region, Icarus, 40 (in press).

(29) Wolfe, R.W. (1979) Orientation of eolian features in the north polar region of Mars: A preliminary assessment (Abstract), Lunar and Planetary Science X, 1364-1366.

(30) Leach, J.H.J. (1979) Dune forms and patterns of wind circulation in the north polar region of Mars (abstract), <u>Second International Colloquium on Mars</u>, NASA CP 2072, 52.

(31) Tsoar, H., R. Greeley, and A.R. Peterfreund (1979) Wind patterns and cyclone formation in the north polar region of Mars: analysis from sand dune morphologies (abstract), <u>Reports to the Planetary Geology Program (1978-1979)</u>; NASA TM 80339, 316-318.

(32) French, R.G., P.J. Gierasch, B. Popp, R. Yerdon (1979) Cloud forms on Mars (abstract), <u>Bulletin of the American Astronomical Society</u>, Vol. 11, No. 3, 572.

(33) Snyder, C.W. (1977) The missions of the Viking Orbiters, <u>J. Geophys. Res.</u>, 82, 3971-3983.

(34) James, P.B., G. Briggs, J. Barnes, and A. Spruck (1979) Seasonal recession of Mars' south polar cap as seen by Viking, <u>J. Geophys. Res.</u>, 84, 2889-2922.

(35) Blasius, K.R., J.A. Cutts, and W.J.Roberts (1973) Large scale erosive flows associated with Chryse Planitia, Mars: source and sink relationships, <u>Reports of Planetary Geology Program, 1977-1978</u>, NASA TM 79729, 275-276.

(36) Tsoar, H., R. Greeley, R. Papson, and S. Squyres (1977) Sand dunes of the north polar region of Mars (Abstract), <u>Lunar and Planetary Science X</u>, 1242-1244.

APPENDIX A

List of Viking Orbiter Imagery Used in Research

Viking Mosaic	Frames From Mosaic
211-5269	59B61-80,; 60B21-40.; 61B21-42
211-5270	56B71-90 ; 57B21-40 ; 58B26-42
211-5272	59B31-44 ; 60B01-14 ; 61B01-15 ; 62B22-33
211-5273	56B51-69 ; 57B01-18 ; 58B01-17
211-5283	COMPOSITE
211-5337	77B81-94
211-5359 A,B,C,D,E,F,G,H	COMPOSITES
211-5429	56B91-95 ; 57B41-45 ; 58B43-45 ; 59B81-83
	60B41-45 ; 61B42-44 ; 62B62-64 ; 63B43-45
	65B73-75
211-5431	62B41-62 ; 63B21-42 ; 65B51-72
211-5453	52B61-80 ; 84B01-21 ; 84B3' 43 ; 84B51-55
211-5559	77B21-44 ; 77B51-70 ; 80B11-28 ; 80B31-38
211-5560	76B11-31 ; 76B41-53 ; 76B61-65
211-5562	70B01-17 ; 70B23-35 ; 70B41-45
211-5563	73B11-28 ; 73B41-60 ; 75B51-54
211-5569	50B21-38 ; 69B01-18
211-5572	77B81-94
211-5573	71B11-26 ; 71B41-53 ; 71B61-65
211-5574	82B22,28 ; 82B31-38 ; 83B11-26 ; 83B31-44
	83B51-62
211-5575	81B51-74 ; 81B77-96 ; 82B12,14,16,18
211-5576	79B43-63 ; 79B65-76 ; 79B79-83
211-5580	64B01-08 ; 66B01-14 ; 67B01-12
211-5583	72B01-16 ; 72B31-42 ; 72B51-54
211-5584	74B31-44 ; 74B51-57
211-5585	78B11-30 ; 78B41-52 ; 78B61-65
211-5641	488B21-34 ; 487B05-14
211-5718	518B37-52
211-5719	120B21-38 ; 120B41-58 ; 120B61-76
	120B81-94
211-5720	122B01-23 ; 122B31-41 ; 122B51-75
	122B81-91
211-5733	561B74-84
211-5744	525B01-16 ; 541B21-34 ; 544B01-16
211-5746	538B01-16 ; 541B01-14 ; 551B83-98
211-5752	499B41-60 ; 514B41-70

211-5753	518B44-81 ; 560B53-66 ; 560B67-80
	560B82-97
211-5758	538B01-16
211-5765	536B21-36 ; 536B41-56 ; 560B41-60
	560B61-80
211-5776	532B21-36 ; 541B21-36 ; 579B75-94
211-5805	570B01-20 ; 574B01-20 ; 576B01-20
211-5806	579B55-74 ; 580B01-20 ; 582B01-20
211-5808	560B81-98 ; 566B61-80 ; 577B71-90
211-5810	669B01-24 ; 669B25-48
211-5812	710A71-94 ; 714A01-22 ; 717A21-40
211-5814	672B01-24 ; 672B25-48 ; 672B51-72
211-5846	501B01-20
211-5854	676B01-24 ; 676B25-48 ; 676B49-72
211-5857	705B01-20 ; 726A41-57 ; 771A21-30
211-5869	560B41-60
211-5875	801A21-26 ; 801A41-46 ; 804B01-06
	806B21-26
211-5885	753A11-54 ; 756A21-36

Individual Viking Frames Reproduced

070B31-35

505B01-16 ; 505B17-40

514B01-20

516B88-94

518B27-36

523B21-34 ; 523B41-56

524B01-16 ; 524B21-36

525B01-16

531B21-36

532B21-36

538B01-16

541B01-14

544B01-16

551B83-98

560B72-80

576B01-20 ; 576B41-60

580B16-20 ; 580B21-34

669B01-24

APPENDIX B

Computer Programs for Crater Size-Frequency Distributions

```
C
C
C     **********************.*****************************************
C
C     SUBROUTINE CRMOD1.FTN    (CRATER DISTRIBUTION MODULE #1)
C
C     ***************************************************************
C
C
C
C     >>>>>>> CUMULATIVE SIZE-FREQUENCY DISTRIBUTION PLOT <<<<<<<
C
C
C              MIKE BOTTS      2/11/79
C
C
C     COMPLETE SUBROUTINE FOR CALCULATING AND PLOTTING CUMULATIVE
C        SIZE-FREQUENCY DISTRIBUTION DATA (ALONG WITH ERROR BARS).
C
C     OUTPUT INCLUDES TABLE OF VALUES NEEDED FOR PLOTTING CUMULATIVE
C        SIZE-FREC. DISTRIBUTION, AND GRAPH OF VALUES AND ERROR LIMITS.
C
C     INPUT:  D = ARRAY OF UNBINNED CRATER DIAMETERS ARRANGED IN
C                     DESCENDING ORDER
C             N = NUMBER OF CRATERS
C             NDIM = ROW DIMENSION GIVEN 'CUMPLT' IN MAIN PROGRAM
C                     (DIMENSION GIVEN 'BARCUM' SHOULD BE 2*NDIM)
C             A = TOTAL AREA (KM**2) OF CRATER COUNTS
C             XAXIS1 = LOWER BOUND OF X-AXIS
C             XAXIS2 = UPPER BOUND OF X-AXIS
C             YAXIS1 = LOWER BOUND OF Y-AXIS
C             YAXIS2 = UPPER BOUND OF Y-AXIS
C
C     NOTES:  IF LIMITS OF GRAPH ARE NOT KNOWN, SET XAXIS1 AND XAXIS2
C                EQUAL TO 0.0 .PROGRAM PLOT.FTN WILL THEN COMPUTE
C                ITS OWN INCREMENTS.
C             X INCREMENT = (XAXIS2 - XAXIS1)/100.
C             Y INCREMENT = (YAXIS2 - YAXIS1)/50 .
C             (PROGRAM WILL ASK IF YOU DESIRE A REPLOT).
C
C     RETURNS :
C             DIA = DIAMETERS OF CRATERS
C             CUM = CUMULATIVE NUMBER OF CRATERS LARGER OR EQUAL TO
C                     DIAMETER AT THAT POINT
C             DIALOG = LOG (D)
C             CUMLOG = LOG (CUM)
C             ERRLOG = LOG (1ST SET OF ERROR LIMITS)
C             AIRLOG = LOG (2ND SET OF ERROR LIMITS)
C             CUMPLT = 2-COLUMN ARRAY OF MEASURED DATA WHERE:
C                     CUMPLT(I,1) = DIALOG(I)
C                     CUMPLT(I,2) = CUMLOG(I)
C             BARCUM = 2-COLUMN ARRAY OF ERROR BAR DATA WHERE:
C                     BARCUM(I,1) = DIALOG(I)
C                     BARCUM(I,2) = ERRLOG(I)
C                     BARCUM(I+1,1) = DIALOG(I)
C                     BARCUM(I+1,2) = AIRLOG(I)
C             J = DIMENSION VARIABLE OF DIALOG,CUMLOG,ERRLOG,AIRLOG
C
C     SUBROUTINES NEEDED:
C             CUMFRQ.FTN       (CALCULATES VALUES NEEDED FOR PLOT)
C             SQUEEZ.FTN       (PREPARES MEASURED DATA FOR PLOTTING PROGRAMS)
C             SQUISH.FTN       (PREPARES ERROR BAR DATA FOR PLOTTING PROGRAMS
C             PLOT.FTN         (PLOTS DATA + ERROR BARS)
C
C     SISTER PROGRAMS:
C             CRMOD2.FTN       (DIFFERENTIAL SIZE-FREQUENCY PLOT)
C             CRMOD3.FTN       (BINNED RELATIVE SIZE-FREQUENCY PLOT)
```

```
C       -------------------------------------------------------------
        SUBROUTINE CRMOD1(D,N,NDIM,A,XAXIS1,XAXIS2,YAXIS1,YAXIS2,DIA,CUM,
       1DIALOG,CUMLOG,ERRLOG,AIRLOG,CUMPLT,BARCUM,J)
        DIMENSION D(N),DIA(N),DIALOG(N),CUM(N),CUMLOG(N),ERRLOG(N),AIRLOG(N),
       1CUMPLT(NDIM,2),BARCUM(2*NDIM,2)
C       ............................................................
C       CALL ROUTINE FOR CALCULATING CUMS
C
        CALL CUMFRQ(D,N,A,DIA,DIALOG,CUM,CUMLOG,ERRLOG,AIRLOG,J)
C       ............................................................
C       LIST VALUES NEEDED FOR PLOT: D,CUM,DIALOG,CUMLOG,ERRLOG,AIRLOG
C
        WRITE (5,100)
        WRITE (5,120)
        WRITE (5,140)
        WRITE (5,150)
100     FORMAT ('1',72('*'))
120     FORMAT ('0',5X,'CUMULATIVE SIZE-FREQUENCY DISTRIBUTION')
140     FORMAT ('0',72('*'))
150     FORMAT ('0  DIAMETER',5X,'CUM. NO./AREA',5X,'LOG(DIAMETER)'
       1,5X,'LOG(CUM. NO./AREA)',5X,'LOG(ERROR LIMITS)')
        DO 200 K=1,J
        WRITE (5,180) DIA(K),CUM(K),DIALOG(K),CUMLOG(K),ERRLOG(K),AIRLOG(K)
180     FORMAT (' ',F10.3,8X,G10.3,4X,'!',4X,F10.3,13X,F10.3,3X,2F10.3)
        IF (AIRLOG(K).EQ.-9999.999) AIRLOG(K) = CUMLOG(K)
200     CONTINUE
C       ............................................................
C       PREPARE DATA FOR PLOT
C
        CALL SQUEEZ(DIALOG,CUMLOG,J,NDIM,CUMPLT)
        CALL SQUISH(DIALOG,ERRLOG,AIRLOG,J,2*NDIM,BARCUM,JJ)
C       ............................................................
C       PLOT DATA AND ERROR LIMITS
C
        WRITE (5,300)
        WRITE (5,320)
        WRITE (5,330)
300     FORMAT ('0X = LOG( DIAMETER (KM) )')
320     FORMAT (' Y = LOG( CUMULATIVE NUMBER OF CRATERS PER KM**2 )')
330     FORMAT (' PHI = ( CUM. NO. +- SQRT( CUM. NO. ) ) / AREA')
        CALL PLOT(CUMPLT,J,NDIM,BARCUM,JJ,2*NDIM,XAXIS1,XAXIS2,YAXIS1,YAXIS2)
C       ............................................................
C       ASK FOR REPLOT OF GRAPH
C
490     WRITE (5,500)
500     FORMAT ('$WOULD YOU LIKE TO REPLOT THIS GRAPH?(0=NO,1=YES):')
        READ (5,505) NSER
505     FORMAT (I1)
        IF (NSER.EQ.0) GO TO 600
        WRITE (5,520)
520     FORMAT ('$LIST XMIN,XMAX,YMIN,YMAX: ')
        READ (5,525) XAXIS1,XAXIS2,YAXIS1,YAXIS2
525     FORMAT (4F10.5)
        CALL PLOT(CUMPLT,J,NDIM,BARCUM,JJ,2*NDIM,XAXIS1,XAXIS2,YAXIS1,YAXIS2)
        GO TO 490
600     RETURN
        END
```

```
C
C
C     **********************************************************************
C
C     SUBROUTINE CUMFRQ.FTN   (CALCULATES CUM-SIZE FREQUENCY VALUES)
C
C     **********************************************************************
C
C     MIKE BOTTS       1/31/79
C
C     CALCULATES VALUES NEEDED TO PLOT CUMULATIVE SIZE-FREQUENCY
C         DISTRIBUTIONS ACCORDING TO STANDARDS SUGGESTED BY
C         'STANDARD TECHNIQUES FOR PRESENTATION AND ANALYSIS OF
C         CRATER SIZE-FREQUENCY DATA' (NASA TM-79730).
C
C     INPUT:
C             D(N) = ARRAY OF MEASURED DIAMETERS (KM) OF N CRATERS
C             A = AREA (KM**2) OF TOTAL PICTURES COUNTED
C
C     OUTPUT:
C             DIA(J) = ARRAY OF DIAMETERS HAVING DIFFERENT VALUES
C             DIALOG(J) = LOG( DIA(J) )
C             CUM(J) = CUMULATIVE NO. OF CRATERS LARGER OR EQUAL TO
C                     DIA(J)
C             ERRLOG(J) AND AIRLOG(J) = LOG ( PHI(J) )
C                     PHI(J) = [CUM(J) +- SQRT( CUM(J) )] / A
C             J = TOTAL NO. OF CRATERS WITH DIFFERENT DIAMETERS
C
C     NOTE: ARRAY D MUST LIST DIAMETERS IN DECENDING ORDER FROM
C         D(1) TO D(N). USE SUBROUTINE SORTC.
C
C     NEGATIVE INFINITY MARKER = -9999.999 .
C
C
C     ------------------------------------------------------------------
      SUBROUTINE CUMFRQ(D,N,A,DIA,DIALOG,CUM,CUMLOG,ERRLOG,AIRLOG,J)
      DIMENSION D(N),DIA(N),DIALOG(N),CUM(N),CUMLOG(N),ERRLOG(N),AIRLOG(N)
      M=0
      DO 100 I=1,N
      IF (I.EQ.N) GO TO 60
      IF (D(I).EQ.D(I+1)) GO TO 100
60    M=M+1
C
C     CALCULATE VALUES FOR EACH DIFFERENT DIAMETER
      DIA(M) = D(I)
      DIALOG(M) = ALOG10(D(I))
      C = 1.0 * FLOAT(I)
      CUM(M) = C/A
      CUMLOG(M) = ALOG10(CUM(M))
      ERRLOG(M) = ALOG10((C + SQRT(C))/A)
      IF (I.GT.1) GO TO 90
      AIRLOG(M) = -9999.999
      GO TO 100
90    AIRLOG(M) = ALOG10((C- SQRT(C))/A)
100   CONTINUE
      J=M
      RETURN
      END
```

54

```
C       ***********************************************************************
C
C       SUBROUTINE SORTC.FTN    (SORTS COLUMNS OF AN ARRAY)
C
C       ***********************************************************************
C
C       MIKE BOTTS      1/31/79
C
C       SORTS ELEMENTS OF EACH COLUMN OF ARRAY A(N,M) INTO DESCENDING ORDER
C         FROM TOP TO BOTTOM AND RETURNS AS APRIME(N,M)
C
C       N = ACTUAL NUMBER OF ROWS IN ARRAY A
C       M = ACTUAL NUMBER OF COLUMNS IN ARRAY A
C       NDIM = ROW DIMENSION GIVEN ARRAY A IN MAIN PROGRAM
C
C       ------------------------------------------------------------------
        SUBROUTINE SORTC(A,N,NDIM,M,APRIME)
        DIMENSION A(NDIM,M),APRIME(NDIM,M)
        DO 20 I=1,N
        DO 20 J=1,M
        APRIME(I,J) = A(I,J)
20      CONTINUE
        L=N-1
        DO 100 K=1,L
        DO 100 J=1,M
        DO 100 I=1,N
        IF(I.EQ.N) GO TO 100
        IF(APRIME(I,J).LE.APRIME(I+1,J)) GO TO 50
        GO TO 100
50      TEMP = APRIME(I,J)
        APRIME(I,J) = APRIME(I+1,J)
        APRIME(I+1,J) = TEMP
100     CONTINUE
        RETURN
        END




C       ***********************************************************************
C
C       SUBROUTINE SQUEEZ.FTN    (SQUEEZES 2 ARRAYS INTO 1 ARRAY)
C
C       ***********************************************************************
C
C       MIKE BOTTS      2/1/79
C
C       TURNS 2 ONE-COLUMN ARRAYS INTO 1 TWO-COLUMN ARRAY.
C            XY(I,1) = X(I)
C            XY(I,2) = Y(I)
C
C       I = ACTUAL NUMBER OF X AND Y VALUES
C       NDIM = ROW DIMENSION GIVEN XY IN MAIN PROGRAM
C
C       GOOD FOR PREPARING DATA FOR SUBROUTINE PLOTER.FTN.
C
C       ------------------------------------------------------------------
        SUBROUTINE SQUEEZ(X,Y,I,NDIM,XY)
        DIMENSION X(I), Y(I), XY(NDIM,2)
        DO 100 J=1,I
        XY(J,1) = X(J)
        XY(J,2) = Y(J)
100     CONTINUE
        RETURN
        END
```

```
C    ****************************************************************
C
C    SUBROUTINE SQUISH.FTN    (SQUISHES 2 UNEQUAL ARRAYS INTO 1 ARRAY)
C
C    ****************************************************************
C
C    MIKE BOTTS      2/2/79
C
C    SPECIAL ROUTINE NEEDED TO PUT ERROR BAR DATA INTO A 2-COLUMN
C        REQUIRED BY SUBROUTINE PLOTER.FTN.
C
C    VALUE(J) = VALUE PLOTTED ON X AXIS (SAME AS X VALUE FOR REAL
C                   DATA POINTS).
C    ERR1(J) = ONE SET OF ERROR BAR LIMITS
C    ERR2(J) = OTHER SET OF ERROR BAR LIMITS
C    J = ACTUAL NUMBER OF 'VALUE' POINTS
C    NDIM = ROW DIMENSION GIVEN 'BAR' IN MAIN PROGRAM
C
C    RETURNS BAR(JJ,2) WHERE JJ = J*2 AND:
C           BAR(1,1) = VALUE(1)          BAR(1,2) = ERR1(1)
C           BAR(2,1) = VALUE(1)          BAR(2,2) = ERR2(1)
C           BAR(3,1) = VALUE(2)          BAR(3,2) = ERR1(2)
C           BAR(4,1) = VALUE(2)          BAR(4,2) = ERR2(2)
C                  .                            .
C                  .                            .
C                  .                            .
C           BAR(JJ,1) = VALUE(J)         BAR(JJ,2) = ERR2(J) .
C
C
C    USED BY MAIN PROGRAM CRPLOT.FTN (CRATER PLOT) WHICH PRODUCES
C        CRATER SIZE-FREQUENCY PLOTS WITH ERROR BARS.
C
C    ----------------------------------------------------------------
     SUBROUTINE SQUISH(VALUE,ERR1,ERR2,J,NDIM,BAR,JJ)
     DIMENSION VALUE(J),ERR1(J),ERR2(J),BAR(NDIM,2)
     JJ = J*2
     N=0
     DO 100 I=1,J
     N=N+1
     BAR(N,1) = VALUE(I)
     BAR(N,2) = ERR1(I)
     N=N+1
     BAR(N,1) = VALUE(I)
     BAR(N,2) = ERR2(I)
100  CONTINUE
     RETURN
     END
```

```
C     ********************************************************************
C
C     SUBROUTINE PLOT.FTN     (PLOTS 2 SETS OF DATA ON ONE GRAPH)
C
C     ********************************************************************
C
C     MIKE BOTTS      2/16/79
C
C     MODIFIED VERSION OF DAVIS' PLOTER.FTN #: GRAPH BOUNDARIES CAN NOW
C         BE GIVEN BY USER OR CALCULATED BY PROGRAM. IF CALCULATED BY
C         PROGRAM, ROUTINE NOT GUARANTEED TO GIVE 'CLEAN' INTERVALS.
C     # (DAVIS, J.C. (1973),'STATISTICS & DATA ANALYSIS IN GEOLOGY',PG  211
C
C     PLOTS TWO VARIABLES ON ONE GRAPH. IF THE TWO VARIABLES CONSIST OF
C         DATA + ERROR LIMITS, IT IS SUGGESTED THAT THE DATA ARRAY = Q1,
C         AND THE ERROR ARRAY = Q2.
C
C     INPUT:
C             Q1 = FIRST SET OF VARIABLES TO BE PLOTTED, WHERE
C                     Q1(I,1) = VALUE PLOTTED IN X DIRECTION
C                     Q1(I,2) = VALUE PLOTTED IN Y DIRECTION
C             Q2 = SECOND SET OF VARIABLES TO BE PLOTTED
C             N1 = ACTUAL NUMBER OF ROWS OF Q1
C             N2 = ACTUAL NUMBER OF ROWS OF Q2 (SET = 0 IF ONLY ONE DATA
C                     SET IS TO BE PLOTTED)
C             N3 = ROW DIMENSION GIVEN Q1 IN MAIN PROGRAM
C             N4 = ROW DIMENSION GIVEN Q2 IN MAIN PROGRAM
C             XAXIS1 = LOWER BOUND OF X AXIS
C             XAXIS2 = UPPER BOUND OF X AXIS
C             YAXIS1 = LOWER BOUND OF Y AXIS
C             YAXIS2 = UPPER BOUND OF Y AXIS
C
C     NOTES:  IF YOU WISH BOUNDARIES CALCULATED FOR YOU , SET XAXIS1 AND
C                     XAXIS2 EQUAL TO 0.0 .
C             IF YOU WISH TO GIVE YOUR OWN BOUNDARIES, NOTE THAT :
C                     X INCREMENT = (XAXIS2 - XAXIS1)/100
C                     Y INCREMENT = (YAXIS2 - YAXIS1)/50 .
C
C     OUTPUT:
C             * = 1ST DATA SET
C             _ = 2ND DATA SET
C             O = OVERLAPPING POINT OF 1ST & 2ND SETS
C
C     ------------------------------------------------------------------
      SUBROUTINE PLOT(Q1,N1,N3,Q2,N2,N4,XAXIS1,XAXIS2,YAXIS1,YAXIS2)
      DIMENSION Q1(N3,2),Q2(N4,2),IOUT(101),XX(11)
      DATA IBLNK/' '/,II/'I'/,IPLUS/'+'/,IBAR/'_'/,IMINUS/'-'/,ISTAR/'*'/
      DATA IO/'O'/
C
C     IF XAXIS1 AND XAXIS2 = 0.0 CALCULATE BOUNDARIES AND INCREMENTS
C
      NX1 = INT(XAXIS1)
      NX2 = INT(XAXIS2)
      IF (NX1.NE.0.OR.NX2.NE.0) GO TO 100
C     ..........................................................
C     IF BOUNDARIES NOT GIVEN, DETERMINE MAX & MIN
C
C     FIND MAXS AND MINS OF DATA SET Q1
C
      XAXIS1 = Q1(1,1)
      XAXIS2 = XAXIS1
      YAXIS1 = Q1(1,2)
      YAXIS2 = YAXIS1
      DO 50 J=1,N1
      IF (Q1(J,1).LT.XAXIS1) XAXIS1=Q1(J,1)
```

```
      IF (Q1(J,1).GT.XAXIS2) XAXIS2=Q1(J,1)
      IF (Q1(J,2).LT.YAXIS1) YAXIS1=Q1(J,2)
      IF (Q1(J,2).GT.YAXIS2) YAXIS2=Q1(J,2)
90    CONTINUE
      IF (N2.EQ.0) GO TO 100
C
C     FIND MAXS AND MINS OF DATA SET Q2
C
      DO 70 J=1,N2
      IF (Q2(J,1).LT.XAXIS1) XAXIS1=Q2(J,1)
      IF (Q2(J,1).GT.XAXIS2) XAXIS2=Q2(J,1)
      IF (Q2(J,2).LT.YAXIS1) YAXIS1=Q2(J,2)
      IF (Q2(J,2).GT.YAXIS2) YAXIS2=Q2(J,2)
70    CONTINUE
C     ..............................................................
C     CALCULATE INCREMENTS
C
100   DX = (XAXIS2 - XAXIS1)/100.
      DY = (YAXIS2 - YAXIS1)/50.
C     ..............................................................
C     GET GRAPH LINES AND DIVISIONS SET UP
C
      WRITE (5,103)
103   FORMAT ('OY-AXIS',//)
      Y = YAXIS2
      DO 500 I=1,51
      IF (MOD(I-1,5).EQ.0) GO TO 120
      DO 110 J=1,101
      IOUT(J) = IBLNK
      IF (MOD(J-1,10).EQ.0) IOUT(J)=II
110   CONTINUE
      GO TO 140
120   DO 130 J=1,101
      IOUT(J) = IMINUS
      IF (MOD(J-1,10).EQ.0) IOUT(J) = IPLUS
130   CONTINUE
C     ..............................................................
C     PREPARE DATA SET Q1 FOR PLOTTING
C
140   DO 150 J=1,N1
      IY = NINT( (Q1(J,2) - YAXIS1)/ DY ) + 1
      IF ((52-I).NE.IY) GO TO 150
      IX = NINT( (Q1(J,1) - XAXIS1)/ DX ) + 1
      IOUT(IX) = ISTAR
150   CONTINUE
C     ..............................................................
C     PREPARE DATA SET Q2 FOR PLOTTING
C
      IF (N2.LE.0) GO TO 200
      DO 160 J=1,N2
      IY = NINT( (Q2(J,2) - YAXIS1)/ DY ) + 1
      IF ((52-I).NE.IY) GO TO 160
      IX = NINT( (Q2(J,1) - XAXIS1)/ DX ) + 1
      IF (IX.GT.100) IX = 100
      IF (IOUT(IX).EQ.IO) GO TO 160
      IF (IOUT(IX).EQ.ISTAR) GO TO 155
      IOUT(IX) = IBAR
      GO TO 160
155   IOUT(IX) = IO
160   CONTINUE
C     ..............................................................
C     PLOT ONE LINE OF PLOT
C
200   IF (MOD(I-1,5).NE.0) GO TO 300
      WRITE (5,250) Y,IOUT
250   FORMAT (1X,F10.5,1X,101A1)
```

```
        Y = Y-5.0*DY
        GO TO 500
300     WRITE (5,350) IOUT
350     FORMAT (12X,101A1)
500     CONTINUE
C
C       .............................................................
C     . PRINT BOTTOM LEGEND
C
        XXX = XAXIS1
        DO 600 I=1,11
        XX(I) = XXX
        XXX = XXX + 10.0*DX
600     CONTINUE
        WRITE (5,700) (XX(I),I=1,11,2)
700     FORMAT (8X,6(F10.5,10X))
        WRITE (5,800) (XX(I),I=2,10,2)
800     FORMAT (18X,5(F10.5,10X))
        WRITE (5,900)
900     FORMAT (50X,'X-AXIS')
        RETURN
        END
```

APPENDIX C

Crater Size-Frequency Data

<u>Bulbous Ground</u> :   72°N, 290°W

    frames used :   538B03,538B05,538B08,538B09,538B12

    total area :   5419.107 km²

    number of craters :   156

<u>diameter</u> (km)	<u>cumulative no./area</u> (km^{-2})
19.968	.133 X 10^{-3}
5.233	.266
2.319	.399
2.093	.532
2.092	.665
2.000	.798
1.943	.931
1.542	.106 X 10^{-2}
1.495	.133
1.469	.146
1.395	.160
1.345	.186
1.306	.200
1.248	.213
1.196	.240
1.175	.266
1.160	.279
1.121	.319
1.101	.333
1.077	.373
1.046	.399
1.015	.439
1.000	.452
.998	.466
.972	.546
.955	.599
.897	.652
.881	.719
.870	.732
.858	.745
.822	.785
.797	.798
.780	.812
.768	.825
.748	.905
.734	.971
.725	.102 X 10^{-1}
.702	.106
.692	.108
.691	.113
.673	.114

(continued)

diameter (km)	cumulative no./area (km^{-2})
.661	.121 X 10^{-1}
.652	.124
.624	.125
.615	.130
.614	.132
.609	.133
.598	.142
.587	.150
.580	.157
.538	.162
.523	.164
.514	.166
.507	.169
.468	.170
.462	.172
.461	.176
.449	.188
.441	.196
.435	.200
.390	.204
.385	.206
.384	.209
.374	.213
.367	.214
.362	.216
.312	.228
.308	.229
.307	.237
.299	.244
.294	.250
.290	.253
.234	.262
.231	.267
.230	.273
.224	.279
.220	.283
.217	.285
.159	.286
.156	.294
.154	.315
.149	.329
.147	.334
.145	.337
.077	.341
.075	.343
.072	.345

Bulbous Ground :   72°N, 59°W

    frames used :   525B01 - 525B06

    total area :   5400.687 km^2

    number of craters :   97.

diameter (km)	cumulative no./area (km^{-2})
3.166	.185 X 10^{-3}
2.174	.555
1.871	.741
1.594	.130 X 10^{-2}
1.295	.148
1.160	.185
1.151	.222
1.015	.259
1.007	.296
.870	.352
.725	.444
.720	.537
.580	.574
.576	.778
.435	.107 X 10^{-1}
.432	.122
.290	.137
.288	.156
.145	.167
.144	.180

Moderately-mantled Ground :   76°N, 90°W

    frames used : 70B04, 71B61 - 71B64

    total area : 24,344.584 km^2

    number of craters : 71

diameter (km)	cumulative no./area (km^{-2})
12.878	.411 X 10^{-4}
10.231	.822
9.625	.123 X 10^{-3}
6.648	.164
6.576	.205
6.241	.246
5.540	.298
4.818	.329
3.942	.370
3.042	.411
2.847	.452
2.750	.493
2.466	.534
2.200	.575
2.063	.616
1.787	.657
1.650	.698
1.314	.822
1.095	.904
.962	.986
.876	.107 X 10^{-2}
.831	.111
.830	.115
.825	.119
.766	.127
.687	.131
.657	.152
.550	.156
.548	.168
.438 .	.177
.416	.181
.411	.185
.329	.189
.277	.205
.275	.209
.274	.230
.219	.271
.138	.275
.137	.283
.110	.292

Heavily-mantled Ground :   80°N, 65°W

    frames used :   70B06 - 70B10, 70B27 - 70B34

    total area :   55,120,613 km^2

    number of craters : 9
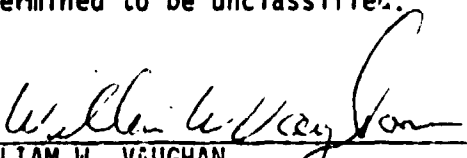
diameter (km)	cumulative no./area (km^{-2})
8.157	.181 X 10^{-4}
4.456	.363
2.232	.544
2.108	.726
.830	.109 X 10^{-3}
.827	.127
.689	.145
.551	.163
.253	.181

APPROVAL

THE STRATIGRAPHIC SEQUENCE OF VOLCANIC AND
SEDIMENTARY UNITS IN THE NORTH POLAR REGION OF MARS

By Michael E. Botts

The information in this report has been reviewed for technical content. Review of any information concerning Department of Defense or nuclear energy activities or pr grams has been made by the MSFC Security Classification Officer. This report, in its entirety, has been determined to be unclassified.

WILLIAM W. VAUGHAN
Chief, Atmospheric Sciences Division

CHARLES A. LUNDQUIST
Director, Space Sciences Laboratory